Seismicity during lateral dike propagation: Insights from new data in the recent Manda Hararo-Dabbahu rifting episode (Afar, Ethiopia)

Raphael Grandin, E. Jacques, A. Nercessian, A Ayele, C. Doubre, A. Socquet, D. Keir, M. Kassim, A. Lemarchand, G. C. P. King

Geochemistry Geophysics Geosystems G3

Article
Volume 12, Number 4
1 April 2011
Q0AB08, doi:10.1029/2010GC003434
ISSN: 1525-2027

Published by AGU and the Geochemical Society

Seismicity during lateral dike propagation: Insights from new data in the recent Manda Hararo–Dabbahu rifting episode (Afar, Ethiopia)

R. Grandin
École Normale Supérieure, 24 rue Lhomond, Paris F-75005, France (grandin@geologie.ens.fr)

Also at Institut de Physique du Globe de Paris, 1 rue Jussieu, F-75238 Paris CEDEX 05, France

E. Jacques and A. Nercessian
Institut de Physique du Globe de Paris, 1 rue Jussieu, F-75238 Paris CEDEX 05, France

A. Ayele
Institute of Geophysics, Space Science and Astronomy, Addis Ababa University, King George VI Street, Addis Ababa 1176, Ethiopia

C. Doubre
Institut de Physique du Globe de Strasbourg, 5 rue René Descartes, F-67084 Strasbourg, France

A. Socquet
Institut de Physique du Globe de Paris, 1 rue Jussieu, F-75238 Paris CEDEX 05, France

D. Keir
National Oceanography Centre, University of Southampton, Southampton SO14 3ZH, UK

M. Kassim
Geophysical Observatory of Arta, BP 1888, Arta, Djibouti

A. Lemarchand and G. C. P. King
Institut de Physique du Globe de Paris, 1 rue Jussieu, F-75238 Paris CEDEX 05, France

[1] Seismicity released during lateral dike intrusions in the Manda Hararo–Dabbahu Rift (Afar, Ethiopia) provides indirect insight into the distribution and evolution of tensile stress along this magma-assisted divergent plate boundary. In this paper, 5 dike intrusions among the 14 that form the 2005–present rifting episode are analyzed with local and regional seismic data. During dike intrusions, seismicity migrates over distances of 10–15 km at velocities of 0.5–3.0 km/h away from a single reservoir in the center of the rift segment, confirming the analogy with a slow spreading mid-ocean ridge segment. Comparison with geodetic data shows that the reservoir is located 7 km down rift from the topographic summit of the axial depression. Dikes emplaced toward the north are observed to migrate faster and to be more voluminous than those migrating southward, suggesting an asymmetry of tension in the brittle-elastic lithosphere. Seismicity during dike injections is concentrated near the propagating crack front. In contrast, faults and fissures in the subsurface appear to slip or open aseismically coeval with the intrusions. The seismic energy released during dike intrusions in the Manda Hararo Rift appears to be primarily modulated by the local magnitude of differential tensile stress and marginally by the rate of stress change induced by the intrusion. The low level of seismic energy accompanying dike intrusions, despite their significant

volumes,is likely an indicator of an overall low level of tension in the lithosphere of this nascent plate boundary.

Components: 16,000 words, 10 figures, 1 table.

Keywords: dike intrusion; mechanics of the lithosphere; mid-ocean ridge.

Index Terms: 7245 Seismology: Mid-ocean ridges; 1242 Geodesy and Gravity: Seismic cycle related deformations (6924, 7209, 7223, 7230); 8010 Structural Geology: Fractures and faults.

Received 11 November 2010; **Revised** 21 February 2011; **Accepted** 8 March 2011; **Published** 27 April 2011.

Grandin, R., E. Jacques, A. Nercessian, A. Ayele, C. Doubre, A. Socquet, D. Keir, M. Kassim, A. Lemarchand, and G. C. P. King (2011), Seismicity during lateral dike propagation: Insights from new data in the recent Manda Hararo–Dabbahu rifting episode (Afar, Ethiopia), *Geochem. Geophys. Geosyst.*, *12*, Q0AB08, doi:10.1029/2010GC003434.

Theme: Magma-Rich Extensional Regimes
Guest Editors: R. Meyer, J. van Wijk, A. Breivik, and C. Tegner

1. Introduction

[2] Dike intrusion is one of the main processes of crustal accretion along divergent plate boundaries, in particular at mid-ocean spreading ridges [e.g., *Delaney et al.*, 1998; *Curewitz and Karson*, 1998]. At slow spreading mid-ocean ridges (full spreading rate: 2–5 cm/yr), magma ascending from the asthenosphere is often focused in the middle of the second-order spreading segments [e.g., *Lin et al.*, 1990; *Smith and Cann*, 1999]. After a temporary storage in a crustal reservoir, melts are then redistributed along the rift by diking, consisting in the horizontal migration of magma [e.g., *Callot and Geoffroy* 2004] along a laterally propagating rupture [e.g., *Abdallah et al.*, 1979; *Einarsson and Brandsdóttir*, 1980]. Dike intrusions are clustered in time, and are typically concentrated in periods of intense magmatic and tectonic activity called "rifting episodes", that last for several months or years, and are separated by long recurrence times (10^2–10^3 yr) [*Björnsson*, 1985]. During an individual rifting episode, several dikes may be emplaced at intervals of a few weeks/months, progressively accommodating the tectonic strain deficit accumulated since the previous rifting episode [*Arnott and Foulger*, 1994; *Buck et al.*, 2006; *Grandin et al.*, 2010b].

[3] From a mechanical point of view, magma is intruded in a dike in response to the existence of a differential tensile stress in the uppermost, brittle part of the lithosphere, and dike intrusions result in a reduction of this differential stress [e.g., *Pollard et al.*, 1983; *Rubin and Pollard*, 1987; *Buck*, 2006; *Grandin et al.*, 2010b, also Elastic thickness control of lateral dyke intrusion at mid-ocean ridges, submitted to *Earth and Planetary Science Letters*, 2011]. Intrusion dynamics reflect an imbalance between magma pressure within the dike P_m and the magnitude of the least compressive principal stress σ_3, corresponding usually to the component of the stress tensor normal to the dike. Locally, the difference between the two terms is defined as the driving pressure $P_d = P_m - \sigma_3$, whose initial (positive) value at the onset of intrusion should control the swiftness of the intrusion.

[4] When magma is intruded into a dike, a swarm of small- to moderate-sized earthquakes (i.e., with $M < 6$) is commonly observed, which provides indirect evidence for occurrence of a rifting event [e.g., *Sykes*, 1970; *Solomon et al.*, 1988]. Because rupture propagation generally occurs unidirectionally along a vertical plane, the process of Mode I opening during a dike intrusion is in many aspects similar to that of Mode II fracture during a strike-slip earthquake [*Pollard and Segall*, 1987; *Rubin*, 1992]. The major difference with "dry" seismogenic rupture is that dike intrusions are slow events, because the velocity of propagation (of the order of 1 km/h *versus* 1 km/s for earthquake rupture) is limited by viscous resistance of magma during transport from the source reservoir to the crack tip [*Spence and Turcotte*, 1985; *Lister and Kerr*, 1991]. As a consequence, propagation of a dike can be considered nearly aseismic. Also, the lack of large seismic events coeval with a dike intrusion is partly related to the high geothermal gradient within volcanic areas, such as at magma-assisted divergent

plate boundaries, where the crustal seismogenic layer is thin.

[5] Nevertheless, stress perturbation within the host rock surrounding the dike releases a small amount of seismic energy, which may be monitored in order to indirectly capture the dynamics of dike emplacement. Using such a method, the first convincing examples of horizontal dike migration were derived from observations made during the Krafla 1975–1984 rifting episode (Iceland), in an oceanic rift segment along the Icelandic section of the mid-Atlantic ridge [*Brandsdóttir and Einarsson*, 1979; *Einarsson and Brandsdóttir*, 1980]. Migration velocities of ~1–2 km/h directed away from a single crustal magma reservoir located at the center of the segment, sustained for a few tens of hours, were deduced from seismic data [e.g., *Tryggvason*, 1984; *Björnsson*, 1985].

[6] More recently, examples of a lateral propagation of seismicity linked with dike emplacement at the axes of various mid-ocean ridge segments with different spreading rates have been reported: in the intermediate spreading Juan de Fuca and Gorda ridges (NE Pacific) [e.g., *Fox*, 1995; *Tolstoy et al.*, 2006; *Dziak et al.*, 2007], the slow spreading mid-Atlantic ridge [*Dziak et al.*, 2004], and possibly in the Gakkel (Arctic Ocean) and Mohns (Norwegian sea) ultraslow spreading ridges [*Blackman et al.*, 2000; *Tolstoy et al.*, 2001]. Unfortunately, the remoteness of oceanic environments has so far hindered deployment of multidisciplinary monitoring devices in these regions, limiting the information content of these small dike-induced earthquakes that could only be recorded by sparse hydrophone or ocean bottom seismometer networks [e.g., *Tolstoy et al.*, 2006]. Nevertheless, the issue of a large distance between a seismically active region and available seismic sensors is not limited to oceanic environments, and was also faced during the two recent and unexpected dike intrusions of short duration (a few days/weeks) that occurred in the continental contexts of Tanzania (2007 Gelai) [*Calais et al.*, 2008; *Baer et al.*, 2008], and Saudi Arabia (2009 Harrat Lunayyir) [*Baer and Hamiel*, 2010; *Pallister et al.*, 2010]. Resolving this problem by focusing on specific spreading segments where dike intrusions are likely to occur in the future, is currently one of the objectives of various research programs (e.g., Ridge 2000 program, 2000, http://www.ridge2000.org; MoMAR project, 2005, http://www.ipgp.fr/rech/lgm/MOMAR/).

[7] Since September 2005, a rifting episode in the Manda Hararo–Dabbahu Rift (MHR) of the Afar volcanic province, including 14 dike intrusions, has been providing scientists with the opportunity to exploit an exceptional geodetic data set, combined with seismological observations gathered by regional and local networks, within the framework of the projects "Dynamics of Rifting in Afar" (DoRA) [*Doubre et al.*, 2009], the 2005–2006 Boina Urgency Project, the 2007–2009 Afar Rift Consortium (http://www.see.leeds.ac.uk/afar), and 2007–2009 Seismic Experiment in the Afar Rift (SEARIFT) [e.g., *Ebinger et al.*, 2010; *Keir et al.*, 2011]. This rifting episode is the first to occur on land since the rifting episodes of Krafla (1974–1985, Iceland) and Asal (1978, Afar, Djibouti) [e.g., *Abdallah et al.*, 1979; *Ruegg et al.*, 1979; *Cattin et al.*, 2005]. The available geodetic data set covering the 2005–present Manda Hararo–Dabbahu rifting episode, mainly interferometric synthetic aperture radar data (InSAR), has allowed the volume, the location and the geometry of each dike intrusion to be precisely constrained. Using this data set, it was shown that the dikes emplaced at various locations along the rift from 2005 to 2010 have involved an enormous volume of magma (in excess of 2 km^3). These observations have confirmed that the current rifting episode is a major plate boundary event, strongly suggesting that the MHR segment is in many respects similar to an oceanic slow spreading segment, albeit at a nascent stage of development [*Wright et al.*, 2006; *Yirgu et al.*, 2006; *Ayele et al.*, 2007; *Rowland et al.*, 2007; *Ebinger et al.*, 2008; *Keir et al.*, 2009; *Hamling et al.*, 2009; *Grandin et al.*, 2009; *Nooner et al.*, 2009; *Ayele et al.*, 2009; *Barisin et al.*, 2009; *Ebinger et al.*, 2010; *Ferguson et al.*, 2010; *Grandin et al.*, 2010a, 2010b; *Hamling et al.*, 2010].

[8] Following *Grandin et al.* [2010b], dike intrusions are numbered from d0 (initial megadike of September 2005), to d13 (last observed dike of May 2010). The migration of seismicity away from a central magma chamber coeval with the two dikes of June and July 2006 (d1 and d2) was reported by *Keir et al.* [2009]. In this paper, we present new seismic data recorded by a small local seismological network that has captured earthquakes associated with three additional dike intrusions in July 2008 (d9), October 2008 (d10) and February 2009 (d11). Our earthquake locations and magnitudes, together with those reported by *Keir et al.* [2009] for the d1 and d2 dikes, and the preliminary results of *Belachew et al.* [2011] for the November 2007 dike (d7), allow us to draw preliminary conclusions on how the variability of the elastic potential energy stored as differential tensile stress along the plate boundary of the MHR may control dike intrusions,

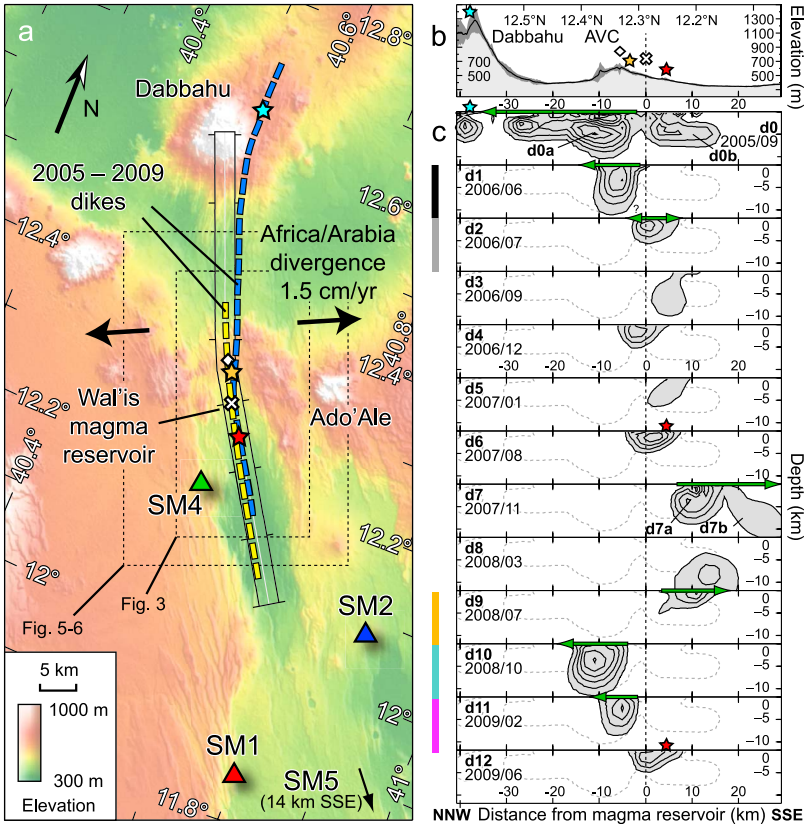

Figure 1. (a) Digital elevation model (DEM) of the Manda Hararo–Dabbahu Rift (MHR), showing the location of September 2005 dike (blue dashed line), 2006–2009 dikes (yellow dashed line), and main source reservoir feeding the dikes (white cross). Triangles indicate the location of seismic stations used to locate earthquakes associated with emplacement of dikes July 2008 (d9), October 2008 (d10), and February 2009 (d11) presented in this study. (b) Cross section in the DEM along the axial profile indicated by a black box in Figure 1a. Horizontal axis is distance along the rift from the central magma reservoir (white cross). White diamond indicates location of the caldera located at the summit of the axial depression. Stars indicate location of eruptions (cyan: silicic explosive coeval with d0; red: basaltic effusive coeval with d6 and d12; orange: basaltic effusive coeval with dike d13). AVC, Ado'Ale Volcanic Complex. (c) Distribution of opening for dikes d0 (September 2005) to d12 (June 2009) deduced from InSAR data [*Grandin et al.*, 2010b]. The dikes are vertical, and each contour represents an opening of 0.5 m on the plane of the dikes, except for megadike d0, where contouring is every 2 m. Green arrows show direction of dike injection deduced from seismicity. Black crosses indicate hypocentral depths of earthquakes associated with dikes d9, d10, and d11 determined in this study.

and to assess the evolution of tectonic stress throughout the duration of the current rifting episode.

2. Data Set and Method

2.1. Network

[9] In November 2007, the Institut de Physique du Globe de Paris (IPGP) and the Institute of Geophysics, Space Science and Astronomy (IGSSA) of the University of Addis Ababa, deployed a telemetered seismological network over the southern tip of the zone affected by the repeated dike intrusions of the MHR (Figure 1a). This network consisted in four short-period stations (bandwidth 0.5–50 Hz) installed as close as possible to the rift axis in order to detect small earthquakes. Unfortunately, the field conditions did not allow us to extend our monitoring network into the inner floor of the rift. Two three-component stations, SM1 and SM4, are located on the western rift shoulder, whereas another three-component station, SM2, lies on a volcano, on the eastern shoulder. A fourth vertical-component station, SM5, is located in the town of Semera. The seismic signals are sent by analog FM radio to Semera where they are continuously digitized and recorded at a sampling rate of 100 Hz.

[10] With this network, numerous volcano-tectonic (VT) events were recorded at the time of three dike

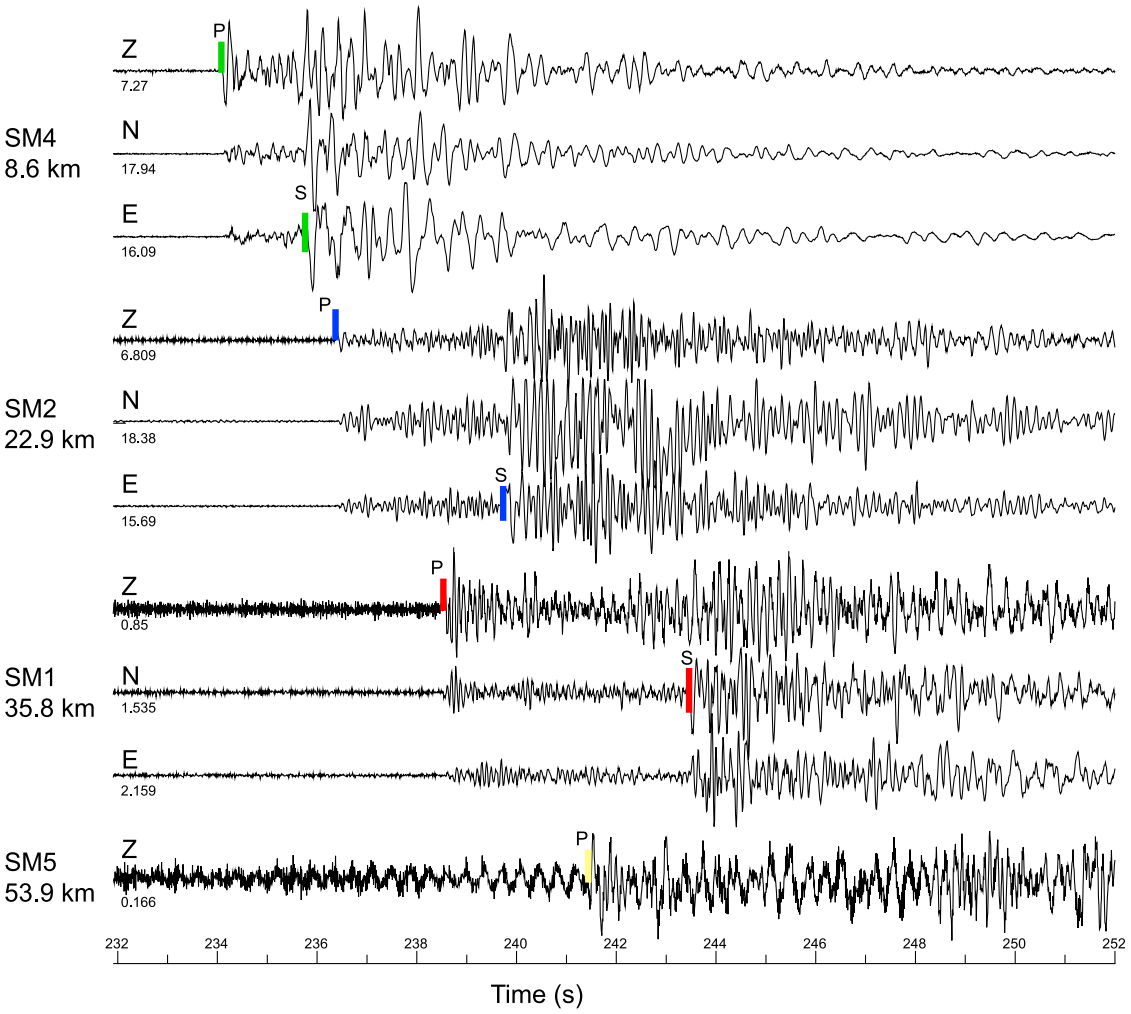

Figure 2. Example of seismic signal recorded by the seismological network. Earthquake of 10 July 2008 at 1002 (UT), with magnitude M_L = 2.7, related to July 2008 dike emplacement, and associated phase pickings, are shown. Epicentral distance from the stations is indicated on the left. Z, N, and E refer to the up-down, north-south, and east-west components of ground velocity at each station, respectively.

intrusions (d9, d10 and d11). Figure 2 shows an earthquake recorded by the network during the sequence related to the July 2008 dike (d9). Phase pickings were performed manually. Estimated uncertainty on phase pickings ranges from 0.02 s for the best defined *P* phases, to 0.20 s for the least constrained arrivals (0.05 s and 0.30 s, respectively, for *S* phases).

[11] For earthquakes with magnitude higher than 2.5, a local magnitude M_L was computed using the amplitude of *S* waves at SM2 and SM4 stations, with the formula $M_L = a_0 + \log(k \times A_d) + a_1 \log(\Delta)$, where k is a static magnification equal to 2800, Δ is the epicentral distance (unit: km), and A_d is the amplitude of ground motion (unit: μm), estimated from $A_d = A_v/\omega$, where A_v is the amplitude of *S* waves read on the horizontal velocity components (unit: μm/s), and ω is the dominant pulsation of *S* waves (unit: rad/s) [*Richter*, 1958]. Values of parameters a_0 and a_1 are derived from seismological studies in Djibouti ($a_0 = -3.2$ and $a_1 = 1.6$) [*Mohamed*, 2009]. For earthquakes with magnitudes higher than 3.5, as the signal was generally saturated at SM2 and SM4, we used the signals recorded at permanent short-period stations of the Geophysical Observatory of Djibouti. For the remaining earthquakes with magnitudes smaller than 2.5, we calculated duration magnitudes M_D using the formula $M_D = b_0 + b_1 \log D + b_2 \Delta$, where D is signal duration (unit: s), and b_0, b_1 and b_2 are parameters derived from *Real and Teng* [1973] ($b_0 = -1.01$, $b_1 = 1.89$ and $b_2 = 0.0009$). The duration magnitude law was then calibrated against local magnitudes for the earthquakes recorded both by our local network and the Djibouti network. Our network detected events

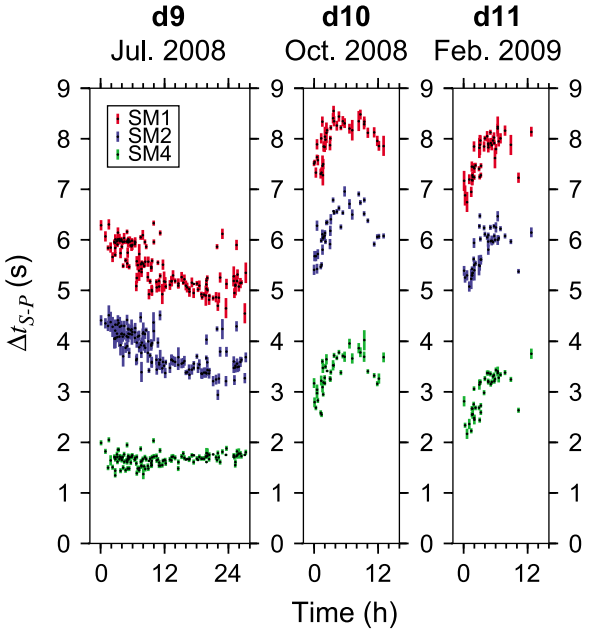

Figure 3. Time difference between first arrivals of *P* and *S* phases (*S*-*P* phase delays Δt_{S-P}) at stations SM1 (red), SM2 (blue), and SM4 (green) for the three dikes d9 (July 2008), d10 (October 2008), and d11 (February 2009). The origin of time axis is set to the time of the first-recorded earthquake of each sequence. The length of the vertical bars corresponds to the uncertainty on phase pickings.

with magnitudes ranging from 1.2 to 4.6, which is slightly less than the magnitude of the events recorded by the regional network discussed by *Keir et al.* [2009].

2.2. Location Method

[12] We proceed to a two-step location inversion in order to assess the impact on earthquake location estimates induced by the unfavorable network geometry used in this study. First, we used a "classical" inversion method, Hypo71 [*Lee and Lahr*, 1975]. We used a 1-D velocity model derived from the seismic refraction profile shot in Ethiopia, between Assaïta and Lake Afdera, in March 1972 (profile V in the study by *Berckhemer et al.* [1975]). We used the central part of the seismic profile, which runs less than 50 km from the zone where the dikes intruded (Model A in Figure S1 in the auxiliary material).[1] A V_P/V_S ratio of 1.77 is estimated following the method described by *Chatelain* [1978] (see also Appendix A by *Jacques et al.* [1999]).

[13] Second, we invert the hypocentral locations directly from the *S*-*P* phase delays available at the three closest stations (Figure 3). We follow the probabilistic approach of *Tarantola and Valette* [1982]. In this scheme, the a posteriori probability density function (p.d.f.) of hypocentral location is calculated by mapping the a priori estimated p.d.f. of the data (i.e., phase picking and associated uncertainty) into the parameter space (i.e., earthquake epicentral location). Travel time of seismic waves (the forward model) is assumed to be perfectly known (perfect theory). Because we invert for three parameters (latitude, longitude and depth), and we use three data points for each earthquake (*S*-*P* phase delays), the problem is mathematically evenly determined, and the inversion always yields a "best" solution. However, the result is very sensitive to errors on the velocity model, particularly for those earthquakes occurring outside the network (dikes d10 and d11), so we chose to limit our analysis to the inversion of two parameters (latitude and longitude, or depth and location along the dike, as explained below). Here, the chosen velocity model consists in a smoothed version of the velocity model used for Hypo71 earthquake locations, with two layers with a gradient of velocity, overlying a half-space of homogeneous velocity (Model B in Figure S1). This method provides a quantification of the errors affecting the estimated earthquake locations, with a result depending both on the assumed errors on phase pickings and the network geometry.

2.3. Epicentral Location Estimate

[14] In a first step, earthquakes were located with Hypo71. Only events recorded at three or more stations and including at least 6 picked arrival times (*P* and *S* phases) were selected for the location inversion. Following this procedure, a total of 326 events have been identified over the period 2008–2009. Among these, 255 events show clear *P* and *S* phases in signals recorded at all three stations SM1, SM2 and SM4 (i.e., three *S*-*P* phase delays are available for these events). Following [*Keir et al.*, 2009], due to the lack of stations directly above the active area, we first constrained the earthquake depth to be fixed to 5 km. We also tested a scenario where the depth of the earthquakes was not constrained, and we found that the results were more stable, with less outliers. This may presumably indicate that at least some earthquakes are located at a depth significantly different from 5 km. In the following, the result of the Hypo71 inversion with unconstrained depth are discussed, with no impact on our conclusions as far as epicentral locations are concerned.

[1] Auxiliary materials are available in the HTML. doi:10.1029/2010GC003434.

[15] In the second step, we use the probabilistic approach described above, with constraints on epicentral locations deduced solely from the 255 available *S-P* phase delays. Epicentral locations are computed with a depth fixed at 5 km to provide a rough estimate of the errors in the earthquake locations, given the geometry of the network, the assumed velocity model, and the estimated errors on phase pickings. The probabilistic approach sheds light on the confidence on the location estimates in the across- and along-dike directions (Figure S2). For the two northerly dikes d10 and d11, the earthquake locations along the strike of the dike (NNW-SSE direction) are estimated to be constrained within less than ±2 km for all earthquakes, and the uncertainty is less than ±1 km in most cases. The uncertainty on the lateral position of earthquakes across the strike of the dikes (WSW-ENE direction) is comparatively larger (±3–4 km on average, and up to ±5 km in the worst cases). In contrast, earthquakes occurring coeval with dike intrusion d9 (July 2008) are better constrained laterally (generally ±2 km).

[16] The locations deduced from the two approaches can be readily compared (Figure S3). Although the assumptions between the two methods differ slightly (inversion with Hypo71 was performed with a non-gradient layered velocity model, free hypocentral depth, and with occasional data from the additional station SM5), we find a very good agreement between the results of the two methods. For the July 2008 dike which occurred less than 10 km from the northern station SM4, 96% of the earthquake locations determined with Hypo71 (i.e., 143 earthquakes out of 149) fall within the 90% confidence region computed solely with *S-P* phase delays in the probabilistic approach. The values are 85% (51/60) and 93% (43/46) for the October 2008 and February 2009 dikes, respectively (Figure S2). Overall, the earthquake location errors deduced from the probabilistic method are likely overestimated, as the breadth of the earthquake swarm deduced from Hypo71 is less than 4 km, suggesting that a ±2 km would be a better suited value for the lateral uncertainty. In contrast, the difference in the along-strike location of earthquakes deduced from the two approaches appears to be smaller (near to ±1 km).

2.4. Hypocentral Depth Estimate

[17] For the two distal dikes of October 2008 (d10) and February 2009 (d11), station-earthquake distances are too large for hypocentral depths to be reliably constrained (epicentral distance to the closest station, SM4, is greater than 15 km, whereas earthquakes are expected to occur above 10 km depth, see Table S1). However, for the July 2008 dike (d9), because the closest station (SM4) is located at an epicentral distance ranging between 6 km and 12 km, we may be able to determine the depth of the earthquakes with some accuracy. To perform this task, we use the probabilistic approach defined above, except that we now invert for the depth of the earthquakes, and, in order to stabilize the inversion, we force the earthquakes to occur exactly along the dike plane determined by the inversion of InSAR data (the two inverted parameters are now the depth and the location along the dike plane).

[18] These results may then be compared with hypocentral depth locations obtained with Hypo71 with the constraint on depth relaxed (Figure 4a). First, as stated above, relaxing the constraint on earthquake depth with Hypo71 gives nearly the same solutions for the epicentral locations as previously found with a fixed depth. Also, the distribution of hypocentral depths with Hypo71 yields an average depth of earthquakes near 5 km, whereas the probabilistic method places the earthquakes at a slightly greater depth, near 6–7 km on average. Accumulation of earthquakes near 5 km obtained with the probabilistic method suggests that the change of the gradient in velocity model B at that depth has an strong impact on the inversion. For the least constrained earthquakes occurring near the northern dike tip, the probabilistic inversion oscillates between two groups of solutions near 7–11 km and 1–2 km depth, whereas Hypo71 converges to an intermediate solution near 6 km depth (Figure 4b), a depth also corresponding roughly to an interface in velocity model A. The shallowest solution with the probabilistic inversion at 1–2 km depth seems to correspond spatially with the locus of maximum opening deduced from InSAR. Yet, earthquakes occurring at that depth, if real, would be poorly constrained (distance to the closest station SM4 is 6 km). In contrast, the rest of the earthquake population seems to be located below the dike, in apparent disagreement with InSAR, although the associated hypocentral depth estimates are more reliable from a geometrical point of view. A crude interpretation could be that most earthquakes are located below the dike, with a few earthquakes located near to the locus of maximum dike aperture.

[19] However, the depth of the dike estimated from InSAR is poorly constrained, and the absolute depth of dike intrusions may well be located several kilometers deeper (although the relative depth of individual dike intrusions is well constrained) [*Grandin*

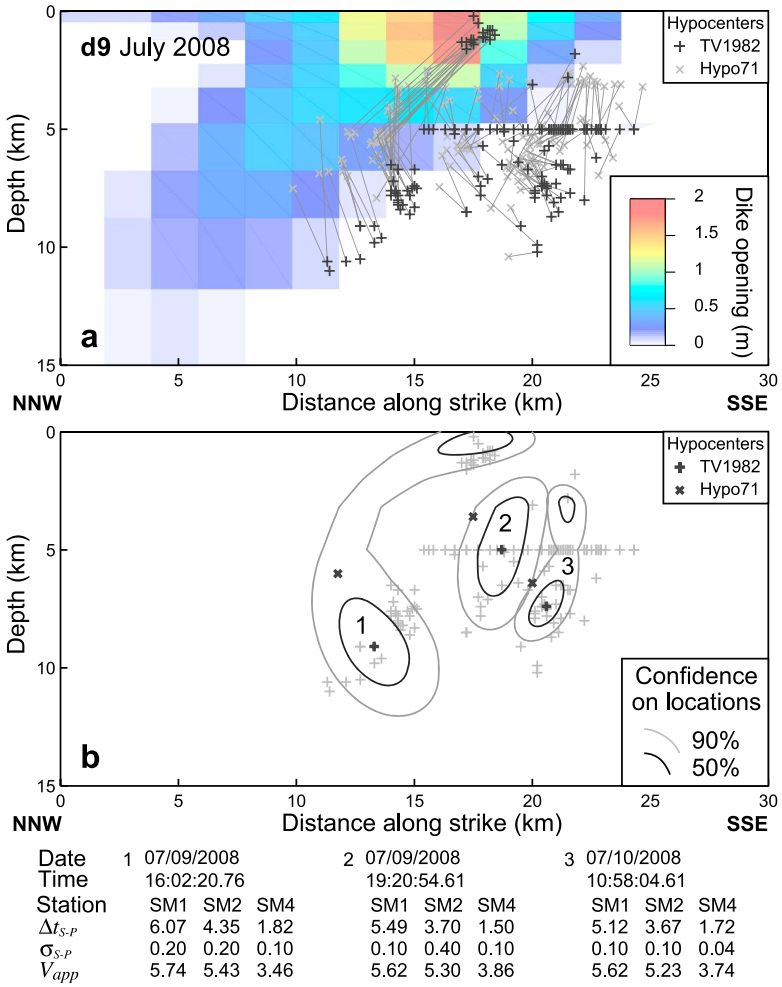

Figure 4. Result of hypocentral depth inversion for earthquakes induced by July 2008 dike intrusion. (a) Hypocenters are plotted along strike, and opening distribution for July 2008 dike is deduced from inversion of InSAR data. The black crosses correspond to the depths deduced when earthquakes are constrained to occur on the plane of dike (see Figure S2 for location). Results of Hypo71 hypocentral locations are indicated by light grey crosses. Small dark grey segments show relationship between locations obtained with the two methods for each event. (b) Examples of distribution of possible hypocentral locations for three earthquakes occurring at different depths and distance along strike. Details on *S-P* phase delays (in s) Δt_{S-P}, assumed errors on phase pickings σ_{S-P}, (in s) and apparent velocity computed at hypocenter V_{app} (in km/s) are indicated at the bottom.

et al., 2010b]. If dike opening in July 2008 actually occurred 2–4 km deeper, a spatial matching between seismicity and the distribution of dike opening would be observed. In that case, the shallow patch of seismicity near 1–2 km depth would likely be interpreted as a spurious result of the inversion, and these earthquakes may be actually located near the region defined by the other group of solutions, at 9 km depth, some 3–4 km toward the north (as suggested by the shape of the contour of 90% confidence on hypocentral depth of event 1 in Figure 4b). The distribution of hypocentral depths deduced from the comparison of Hypo71 and the probabilistic method could therefore be compatible with the alternative interpretation that most earthquakes have occurred at the depth of the dike intrusion, which was likely underestimated by *Grandin et al.* [2010b]. This spatial matching between the dike shape and the location of dike-induced earthquake activity is also supported by the greater depth of earthquakes found near the northern dike tip of the dike (~8 km) than near its southern tip (~5 km), which is consistent with the shallowing of the dike toward the south deduced from InSAR.

3. Results and Discussion

[20] Due to different problems, including disruptions in power supply, we have only been able to

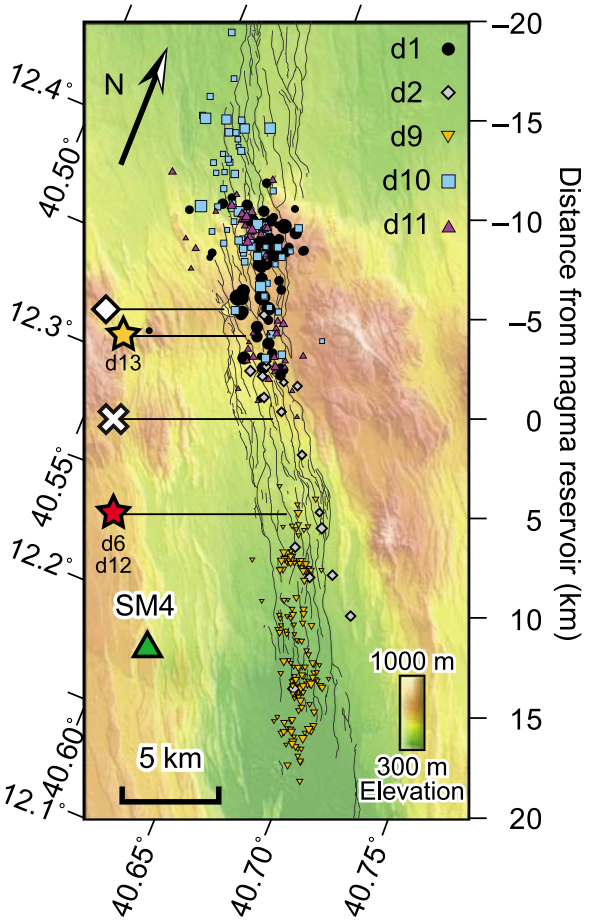

Figure 5. Summary of epicentral locations presented in this study, plotted on a precise DEM of the MHR, and superimposed on the surface trace of faults and fissures that were active during the 2005–present rifting episode [*Grandin et al.*, 2009]. The epicentral locations presented here correspond to the result of the Hypo71 inversion with unconstrained depth. The size of symbols depends on earthquake magnitude. Note the gap in seismic activity near the location of the inferred Wal'is source reservoir (white cross). Stars show the location of basaltic fissural eruptions (red: basaltic effusive coeval with d6 and d12; orange: basaltic effusive coeval with dike d13). The white diamond indicates location of the caldera located at the summit of the axial depression.

use the local seismic network described above to record and locate earthquakes related to three dike intrusions: July 2008 (d9), October 2008 (d10) and February 2009 (d11). Earthquakes induced by the June 2006 (d1) and July 2006 (d2) dike intrusions studied by *Keir et al.* [2009] are also included in this paper for comparison. The epicentral locations associated with each of the five dike intrusions are shown in Figure 5.

3.1. Time Evolution of Seismic Activity

[21] Earthquake activity in the MHR in 2005–2010 appears to be clustered in time and space. During the periods between dike intrusions, little seismicity is detected, and no earthquake could be located near the axis of the MHR. However, this lack of observation does not preclude that small undetected earthquakes may actually occur between dike intrusions, as suggested by observations of continued seismic activity along the rift axis between November 2005 and May 2006 reported by *Ebinger et al.* [2008], as well as evidence for significant microseismicity above the inferred central reservoir of the Asal rift during the current interdiking period reported by *Doubre et al.* [2007b]. Nevertheless, our observations suggest that seismic activity is mainly concentrated during dike intrusions, and is organized in swarms lasting for 24–48 h. The evolution of cumulative Benioff strain released by earthquakes during individual dike intrusions shows a gradual increase of the rate of energy release, followed by a slow decay, with no clear mainshock-aftershock succession (Figure 6). This symmetrical distribution of seismic energy release as a function of time is typical of earthquake swarms, and is compatible with a magmatic origin of seismicity [e.g., *Sykes*, 1970]. The simultaneity between dike opening and seismic activity has already been clearly demonstrated by the abrupt ground displacement measured by continuous GPS stations for dikes d1 and d2 [see *Keir et al.*, 2009, Figure 3]. Furthermore, a dense SAR archive acquired by the ENVISAT satellite has also allowed *Grandin et al.* [2010b] to show that deformation associated with other dike intrusions is likely restricted to a period shorter than ~4 days. These independent constraints strongly suggest that the earthquake swarms are tightly related to the dike intrusions detected with InSAR and GPS.

3.2. Spatial Clustering of Earthquakes

[22] Epicentral locations show that seismicity associated with each dike intrusion is concentrated in an elongated band along the axis of the MHR. Individual swarms have a length of 10–13 km, and a width of 2–4 km (Figure 5). Superimposition with InSAR data shows that the across-axis width of the seismically active region does not extend laterally beyond the limits of the surface ruptures associated with normal faulting above the dike [*Grandin et al.*, 2010b] (Figures 7 and 8). Beyond confirming that dikes are emplaced with a nearly vertical dip, this observation strongly suggests that our

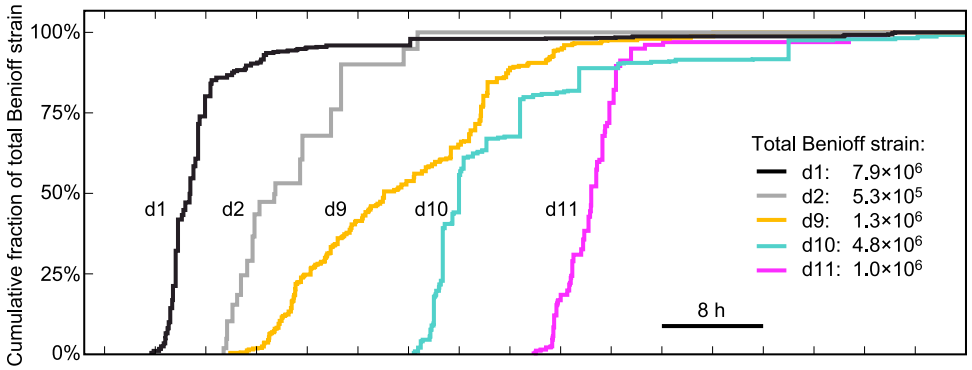

Figure 6. Cumulative Benioff strain as a function of time, calculated from the distribution of seismicity associated with the five dike intrusions discussed in this study. Curves have been scaled vertically to the total amount of Benioff strain (indicated to the right), and shifted horizontally to enable a comparison of the rates of seismic energy release. The Benioff strain B is defined as the square root of radiated seismic energy E_S associated with an earthquake [*Benioff and Richter*, 1951]. The cumulative Benioff strain $\Sigma B(t)$ is a measure of the strain released during a sequence of earthquakes that places more emphasis on the small earthquakes (which are implicitly neglected in a cumulative seismic moment release representation), while simultaneously respecting the hierarchy between small and large earthquakes (which is ignored in a cumulative number of earthquakes count). To calculate E_S (expressed in Nm) from earthquake magnitudes M, we use the Gutenberg-Richter empirical relationship $\log E_S = 3/2 \times M + 4.8$ [*Gutenberg and Richter*, 1956].

absolute epicentral locations are well constrained. This also indicates that seismicity is directly related to stress perturbation in the host rock occurring in the vicinity of the opening dike.

[23] In map view, we observe that, during dike intrusions, earthquakes are concentrated in spatially restricted regions along the dikes. The clusters occur at specific locations along the MHR (Figure 5): (1) two clusters at −9 km and −2 km to the north of the source reservoir are active near the two extremities of dikes d1 and d11, and (2) one cluster near 8 km to the south, is located near the southern end of d2 and the northern end of d9 (Figures 7 and 8). We note a great similarity between patterns of strain energy release for dikes d1 and d11, where two regions of significant seismic energy release along the dike length (−2 km and −9 km) have retained the same location. In contrast, the cluster located at −5 km, which was very active coeval to d1, and may have been involved in generating the seismicity in the first 2 h of intrusion d10, has disappeared in d11. Another possible cluster may be located near −15 km, at the northern tip of dike d10.

[24] A similar clustering of seismic activity during dike intrusions is also observed at Kilauea (Hawaii), and is attributed to the existence of "barriers" caused by local stress concentrations and/or geometric complexities such as jogs or en échelon steps between dike subsegments, separated by shadows of seismicity interpreted as inferred magma reservoirs, or zones of weakness [*Hill*, 1977; *Klein et al.*, 1987]. In the MHR, among the different clusters identified here, the one located near −9 km (12.38°N) seems to correspond to the location of prominent normal faults dissecting the remnants of the Ado'Ale Volcanic Complex (Figure 5). In contrast, the gap in seismic energy release near 0–2 km (~12.29°N) matches with the inferred source magma reservoir for the dikes, and a relative minimum of seismic energy release near −3 km (12.34°N) may be related to the caldera imprinting the summit of the axial topography, a possible indication of an underlying magma reservoir (Figure 5). Similarly, the fissural eruptions of August 2007 (d6), June 2009 (d12) and May 2010 (d13) seem to be located in relative minimas of seismic energy release (the location of the eruptions is indicated by stars in Figures 7c, 7f, 8c, 8f, and 8i). Future studies of the behavior of faults imaged by InSAR during and between dike intrusions should provide more constraints on the relationship between seismicity, magmatism, topography and rift segmentation.

3.3. Migration of Earthquakes

[25] A migration of seismicity along the axis of the MHR is observed during dike intrusions, as witnessed by the progressive change of *S-P* phase delays at individual stations during the swarms (Figure 3). Epicentral determinations show that migration is directed away from a region located

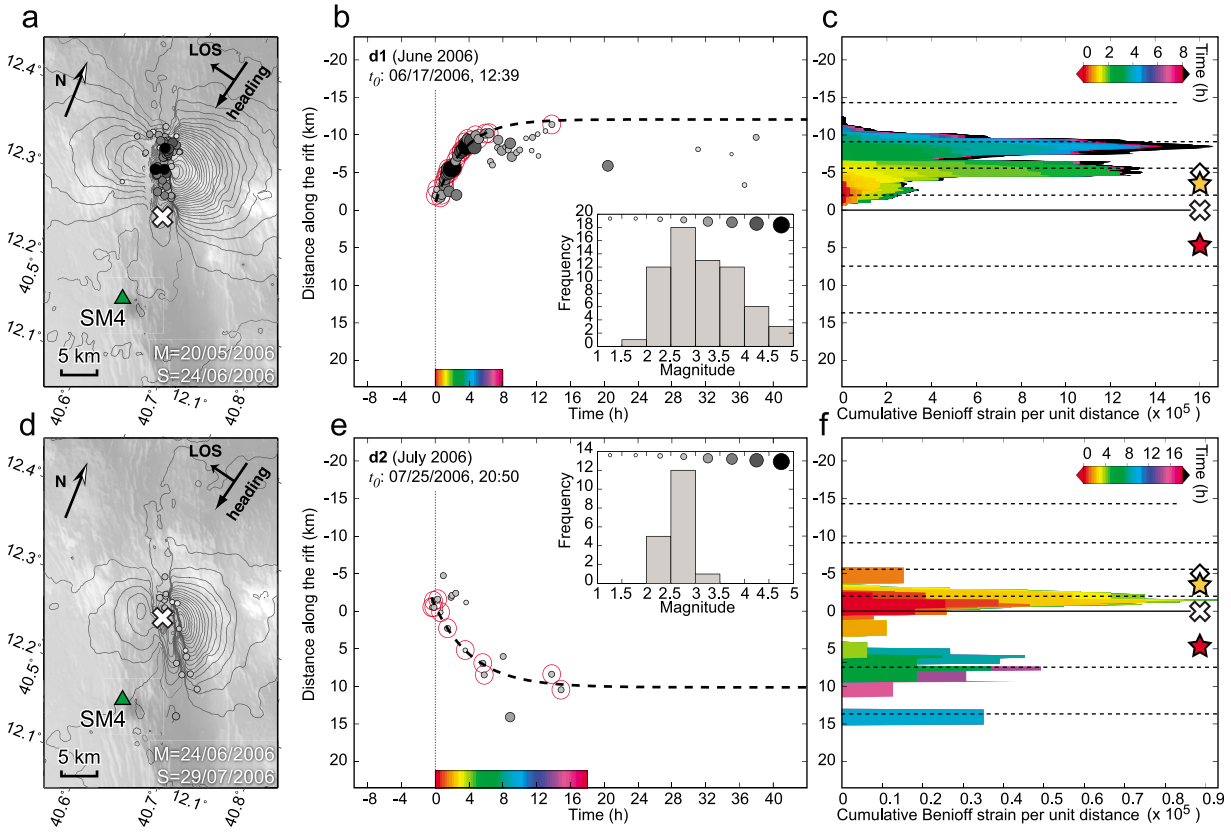

Figure 7. Earthquakes accompanying dike emplacement for (a–c) dikes d1 (June 2006) and (d–f) d2 (July 2006) reported by *Keir et al.* [2009]. Figures 7a and 7d show epicentral locations, with size and grey shading of symbols depending on magnitude. White cross indicates location of source reservoir feeding the dikes, inferred from InSAR and seismicity. Contours represent line-of-sight deformation deduced from InSAR for intervals spanning each dike intrusion. Contours represent increments of 2.8 cm of line-of-sight surface deformation ("fringes") deduced from InSAR data for intervals spanning each dike intrusion. The ground is displaced toward the satellite on the side of the rift closest to the satellite (here, the east), whereas the opposite side of the rift is both uplifted and translated horizontally away from the satellite thus yielding a lower number of fringes, with a reversed polarity. InSAR data were acquired by ESA's Envisat satellite on descending track 464, with incidence angle of ~40° with respect to vertical (arrows show satellite trajectory and look direction). Dates of acquisition of master (M) and slave (S) images are indicated at the lower right corner of each panel [see *Grandin et al.*, 2010b, for details]. Figures 7b and 7e show the distribution of seismicity as a function of time, with respect to onset of migration t_0 (UT), indicated by a vertical dashed line. Earthquakes used for fitting a migration pattern with exponentially decaying velocity (thick dashed curves) are surrounded by a red circle. Inset shows a count of the number of earthquakes as a function of magnitude, indicating magnitude of completeness. Figures 7c and 7f show the distribution of cumulative Benioff strain as a function of distance along the rift from the source reservoir. Benioff strain is averaged in 2 km wide sliding windows. Color scale depends on time (see Figures 7b and 7e for reference). Horizontal dashed lines represent peaks of seismic energy release. Note that the scale for Benioff strain release is different for each panel.

around the latitude 12.29 ± 0.015°N. This latitude does not correspond to the prominent summital caldera at the top of the axial relief, but is rather located ~7 km down rift, toward the SSE (Figure 1). This area coincides with the locus of maximum subsidence deduced from InSAR, associated with the intrusion of the two most distal dikes d7 and d10, which were emplaced to the south and to the north, respectively (Figure 8) [*Grandin et al.*, 2010b]. This area also matches with the location of the inflation signal observed by InSAR in the periods between successive dike intrusions [*Grandin et al.*, 2010a]. These observations strongly suggest that dikes are fed from a single source situated at the center of the rift, which is subsequently refilled with magma during interdiking intervals [*Keir et al.*, 2009; *Grandin et al.*, 2010b].

[26] Migration is generally unidirectional, and occurs both down rift and up rift during the current rifting episode, thus contradicting the hypothesis that

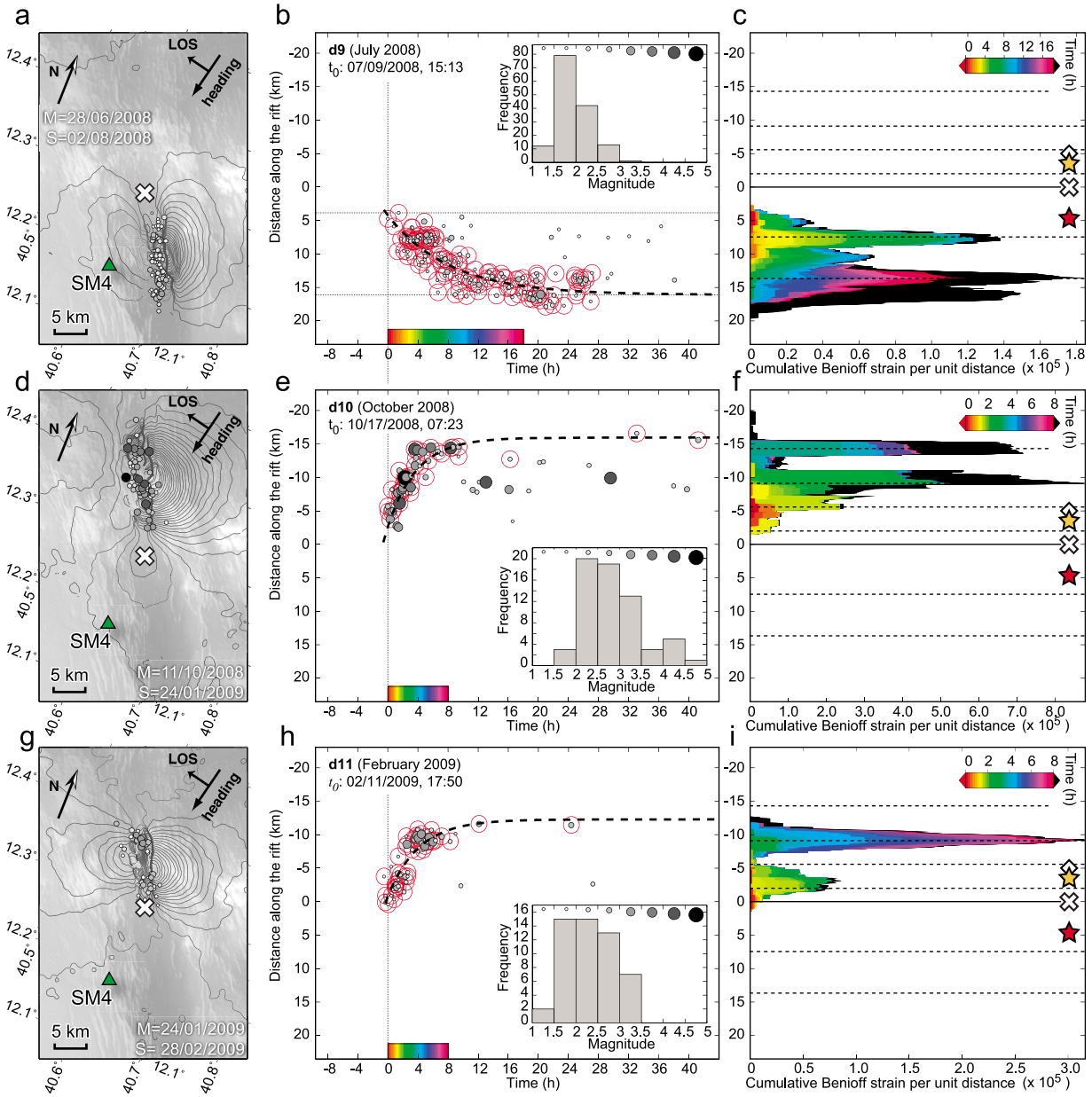

Figure 8. Same as Figure 7 for (a–c) dikes d9 (July 2008), (d–f) d10 (October 2008), and (g–i) d11 (February 2009) presented in this study.

the directivity of lateral dike migration is controlled by the topographic gradient along the axis of the segment, which would otherwise force the dikes to migrate down rift [*Rubin and Pollard*, 1987; *Fialko and Rubin*, 1998; *Buck et al.*, 2006]. Rather, the along-axis thinning of elastic-brittle lithosphere near the segment center, induced by the thermal weakening of the lithosphere due to midsegment focusing of melt, may play a more important role in driving lateral dike injections (Grandin et al., submitted manuscript, 2011). This hypothesis of a thickening of the axial elastic-brittle lithosphere toward segment ends is supported by an analogy with geophysical observations made at similar mid-ocean ridge segments [e.g., *Whitehead et al.*, 1984; *Lin et al.*, 1990; *MacDonald et al.*, 1991; *Hayward and Ebinger*, 1996; *Magde et al.*, 1997; *Doubre et al.*, 2007a; Grandin et al., submitted manuscript, 2011].

[27] A possible indication of an along-axis variation of seismogenic thickness in the MHR may be deduced from the seismic data gathered in the period

Table 1. Dates of the Dikes Discussed in the Text, With Corresponding Volumes V, Maximum Magnitude in the Earthquake Swarm M_{max}, Cumulative Seismic Moment Released During the Swarm M_0, Seismic Efficiency e, Direction of Migration, Length of Swarm l_∞, Characteristic Time Scale of Seismicity Migration τ_W, and Characteristic Velocity of Migration $v_{1/2}$ (Equation (1))

Date	Dike	V[a] (km^3)	M_{max}	M_0 (Nm)	e (%)	Direction of Migration	l_∞ (km)	τ_W (h)	$v_{1/2}$ (km/h)
Sep 2005	d0	1.820	5.5 M_w[b]	3.4×10^{18}	6.22	N and S[c,d]	-	-	0.5–1.0[c,e]
Jun 2006	d1	0.129	4.6 m_b[b]–4.7 M_L[f]	6.1×10^{16}	1.58	N[f]	10.24	3.30	2.24
Jul 2006	d2	0.048	3.5 M_L[f]	3.8×10^{14}	0.03	S[f] (and N ?)	11.73	4.49	1.89
Aug 2007	d6	0.055	-	-	-	-	-	-	-
Nov 2007	d7	0.186	4.7 m_b[b]	3.1×10^{16}	0.56	S[g]	25 ?		
Jul 2008	d9	0.047	3.0 M_L[h]	3.9×10^{14}	0.03	S[h]	12.26	8.22	1.08
Oct 2008	d10	0.198	4.9 M_w[b]–4.6 M_L[h]	2.8×10^{16}	0.47	N[h]	12.21	4.14	2.13
Feb 2009	d11	0.073	3.3 M_L[h]	7.3×10^{14}	0.03	N[h]	12.67	4.07	2.25
Jun 2009	d12	0.044	-	-	-	-	-	-	-

[a] *Grandin et al.* [2010b].
[b] National Earthquake Information Center, U.S. Geological Survey, http://earthquake.usgs.gov/regional/neic/.
[c] *Ayele et al.* [2009].
[d] *Grandin et al.* [2009].
[e] Average migration velocity.
[f] *Keir et al.* [2009].
[g] *Belachew et al.* [2011].
[h] This study.

October 2005–April 2006 (between megadike d0 and d1) by *Ebinger et al.* [2008], who report a decrease in earthquake depths from Dabbahu toward the segment center (see their Figure 7). Unfortunately, as discussed above, difficult access to the field hindered an optimal network configuration, with the consequence that the depths of the earthquakes captured in the MHR are currently not sufficiently constrained to define systematic variations of the seismogenic thickness. In particular, because the closest stations used by *Ebinger et al.* [2008] are located at epicentral distances larger than 30 km for events occurring in the region of emplacement of dikes d1 to d13, hypocentral depth estimations are particularly sensitive to uncertainty on the "average Afar" velocity model used in this study and that of *Jacques et al.* [1999].

[28] One exception to unidirectional propagation may be dike d2, which lies above the source reservoir (Figure 1). In that case, intrusion was likely to be both vertical and horizontal, and possibly horizontally bidirectional, with the earthquakes occurring in the first 4 h hinting at a ~1–2 km northward migration (Figure 7). Unfortunately, interpretation of the migration pattern for this dike is difficult, because only distant stations were operating at the time of the intrusion, so that only 18 small-magnitude earthquakes ($M < 3.5$) could be located [*Keir et al.*, 2009].

[29] During individual earthquake swarms, most of the seismic energy is released during the first 5–20 h of seismic activity, when migration of earthquakes is observed, which we interpret as the duration of the magma intrusion (Figure 6). The average migration velocities for the five dikes studied here are in the range of 0.5–3.0 km/h (Figures 7 and 8), which is consistent with the migration of earthquakes associated with the September 2005 megadike (d0), reported by *Ayele et al.* [2009] (Table 1). These values are similar to those deduced from the study of other dike intrusions in the Krafl Rift during the 1975–1984 rifting episode (~1.6 km/h) [*Brandsdóttir and Einarsson*, 1979; *Einarsson and Brandsdóttir*, 1980], or at the slow and intermediate spreading segments of the mid-ocean ridge system, where such observations have been reported (~1–2 km/h) [*Dziak et al.*, 2007], and are likely to reflect the low viscosity of basaltic melts involved in these intrusions.

[30] Migration velocities are not constant during intrusions, but rather decrease during the intrusion, until the final length of the dike is reached. This suggests a progressive decrease of the horizontal gradient of driving pressure as the dike grows, resulting from a combination of many factors, including pressure decrease in the magma as the material is withdrawn from a source reservoir of finite size [e.g., *Ida*, 1999; *Buck et al.*, 2006; *Rivalta*, 2010], decrease of the magnitude of elastic stress at the crack front as the shape of the dike changes during its growth [e.g., *Taisne and Tait* 2009], and/or an increasing tendency to freezing in the tip region as the dike lengthens and duration of

magma transport, and hence heat loss, increases [e.g., *Spence and Turcotte*, 1985; *Fialko and Rubin*, 1998]. Therefore, migration of seismicity provides important constraints on the dynamics of dike intrusions.

[31] To compare quantitatively the different dike intrusion velocities, we assume that the distribution of seismicity follows an exponential law of time:

$$l(t) = l_\infty\left(1 - e^{-(t-t_0)/\tau_W}\right), \quad (1)$$

where l is dike length measured from the location of the onset of seismicity migration, t_0 is the time of initiation of dike propagation, l_∞ is the asymptotic dike length and τ_W is the characteristic time scale of dike propagation. This law is appropriate to describe the coupling between an overpressurized source reservoir and a laterally growing planar intrusion, assuming conservation of mass [e.g., *Dvorak and Okamura*, 1987; *Lengliné et al.*, 2008; *Rivalta*, 2010]. With the assumption of a constant dike height and thickness during propagation, the dike volume, like the seismicity, follows an exponential evolution. From the above relation, and following an analogy with half-life in radioactive decay, we estimate a characteristic velocity of migration $v_{1/2} = l_\infty/(\tau_W * 2\ \ln(2))$, which corresponds to the time taken by the dike to reach its half-length. We performed a least squares adjustment of the parameters in equation (1) using our data set (Figures 7 and 8). The values of l_∞, τ_W and $v_{1/2}$ are reported in Table 1.

[32] Of particular interest are the characteristic velocities $v_{1/2}$, which range from 1.0 to 2.3 km/h (Table 1). Among the five dikes presented in this study, these velocities appear to be loosely correlated with dike volume (Table 1). This may be attributed to different magnitudes of the driving pressure for the different dikes, with the fastest, most voluminous dikes, corresponding to the greatest magma pressure at onset of dike intrusion [*Lister and Kerr*, 1991; *Mériaux and Jaupart*, 1995]. Yet, preliminary analysis of seismicity associated with dike d7 (November 2007) that propagated toward the south, suggests a slow velocity for this dike [*Belachew et al.*, 2011], despite a volume comparable to that of dike d10, one of the fastest of the migrating dikes. Therefore, the apparent correlation between dike volume and migration velocity highlighted here may be biased by the fortuitous sampling of dikes available for this study, and may not have general significance.

[33] Nevertheless, a key observation is that dikes migrating northward (d1, d10 and d11) are more voluminous and migrated faster than those emplaced southward (d2 and d9). This is in keeping with the observation of *Grandin et al.* [2010b], who showed that during the 2005–2009 sequence of 13 intrusions, dikes emplaced toward the south were generally smaller than those emplaced toward the north, with the notable exception of dike d7 (November 2007), which migrated up to 25 km southward, the greatest distance for all dikes since d0 (September 2005). The asymmetry in opening includes the September 2005 megadike, with a larger peak opening toward the north (6–8 m) than the south (<5 m) [*Grandin et al.*, 2009] (Figure 1c). The authors interpreted this observation as being caused by to the combination of (1) an overall increase of tension stored in the elastic lithosphere at increasing distance from the central magma reservoir and (2) an asymmetry of the distribution of tension, with more differential tensile stress stored in the lithosphere in the north than in the south. The origin of the asymmetry may be related to the history of rifting episodes in the past [*Grandin et al.*, 2009], as observed in Iceland [*Björnsson*, 1985], and/or differences in thickness of the elastic-brittle lithosphere north and south of the magma reservoir (Grandin et al., submitted manuscript, 2011).

3.4. Seismic Moment Release Associated With Dike Intrusions

[34] For each dike, the cumulative seismic moment M_0 released during dike emplacement can be estimated using local magnitudes M_L and duration magnitudes M_D that we have estimated for dikes d9, d10 and d11 on the one hand, and local magnitudes M_L provided by *Keir et al.* [2009] for dikes d1 and d2 on the other hand. Body wave magnitudes m_b or moment magnitudes M_w calculated by NEIC (National Earthquake Information Center) for the largest earthquakes are also available. When comparison is possible, these magnitudes agree within 0.3 units of magnitude. Conversion from magnitudes M (whether M_w, m_b, M_L or M_D) to seismic moment M_0 (expressed in Nm) is performed using the formula $M = 2/3 \times \log M_0 - 6.03$ [*Hanks and Kanamori*, 1979].

[35] As could be expected, the maximum magnitude of earthquakes accompanying dike intrusions is larger for the most voluminous dikes d0, d1 and d10, and lower for the smaller dikes d2 and d9 (Table 1). Yet, as is commonly observed for magma intrusions, most of the deformation during the dike injections of the MHR occurs aseismically [e.g., *Foulger and Long*, 1984; *Pedersen et al.*,

2007]. This includes the megadike d0 of September 2005, which involved a volume of magma in excess of 1 km^3 [*Wright et al.*, 2006; *Ayele et al.*, 2007; *Grandin et al.*, 2009; *Ayele et al.*, 2009]. Seismic moment release among the five dikes presented here spreads across 2 orders of magnitude, whereas dikes volumes differ by a factor less than 4. Including the megadike d0 (September 2005) increases this discrepancy, with a volume greater than that of dike d9 by a factor 39, and a seismic moment release greater by a factor 10,000. This tendency is highlighted by the "seismic efficiency" e, defined here as the ratio between the geodetic moment release M_g and the cumulative seismic moment M_0 released during dike emplacement (multiplied by 100 if expressed in percent). The geodetic moment M_g is here defined as the product of the volume of the dike V and Young's modulus E. Here, we use E = 30 GPa, following *Grandin et al.* [2010b].

[36] Despite uncertainty on the value of the elastic modulus and the possible bias on the estimation of the total seismic moment release resulting from the inhomogeneous seismic data set, we observe that seismic efficiency is very small, with M_g/M_0 spanning between 6% for the September 2005 megadike (d0) and 0.03% for the d2, d9 and d11 dikes (Table 1). This compares well with the July 1978 Krafla dike intrusion (Iceland), which had a seismic efficiency of 0.6% [*Einarsson and Brandsdóttir*, 1980; *Pedersen et al.*, 2007]. In contrast, a seismic efficiency of 40% is observed for the 2000 dike intrusion offshore the Izu peninsula (Japan) [*Toda et al.*, 2002; *Pedersen et al.*, 2007], 55% for the 2007 Gelai dike intrusion (Tanzania) [*Calais et al.*, 2008; *Baer et al.*, 2008], and 14–25% for the 2009 Harrat Lunayyir dike intrusion (Saudi Arabia) [*Baer and Hamiel*, 2010; *Pallister et al.*, 2010].

[37] The overall low seismic efficiency of dike intrusions in the MHR means that most of the strain change induced by intrusion of the dikes does not lead to brittle seismogenic rupture of host rock, and is accommodated by a combination of aseismic slip, tensile opening, ductile deformation, and/or elastic strain not exceeding brittle resistance of rocks. This low seismic efficiency likely reflects host rock that is initially relatively far from the brittle failure envelope, which is consistent with the low background seismic activity observed in the volcanic rift zones of the Afar region [*Rubin and Gillard*, 1998; *Pedersen et al.*, 2007; *Hofstetter and Beyth*, 2003]. Such a low level of tectonic stress may be possibly related to the maturity of this proto-oceanic plate boundary, where plate strength is lower and magma supply rate is higher than in the less evolved continental rift environments mentioned in the above examples [*Solomon et al.*, 1988; *Baer and Hamiel*, 2010].

[38] Among the dikes intruded in the MHR, an apparently greater seismic efficiency is observed for the most voluminous dikes, and a comparatively lower efficiency for smaller intrusions (Table 1). This suggests that the rate of stress perturbation plays an additional role in modulating the amount of seismic energy released during a dike intrusion, which is compatible with the hypothesis that rate-and-state constitutive laws govern the process of earthquake generation [*Dieterich et al.*, 2000; *Toda et al.*, 2002].

[39] Nevertheless, the case of dikes d1 and d11, which exhibit significantly different seismic efficiencies (1.58 % and 0.03 %, respectively) despite similar rates of stress change (within a ratio of 1–2, as inferred from the proxy $V \times v$, where V is dike volume and v is migration velocity), and a location in nearly the same region of the plate boundary (see also section 3.6), may suggest that the importance of the rate of stress change in our data set should be toned down. Rather, the progressive decrease of background tensile stress is more likely to have caused the dramatic decrease of seismic efficiency observed from June 2006 (d1) to February 2009 (d11). This can be deduced from the evolution of normal stress on the vertical plane of the plate boundary during the 2005–present rifting episode in response to the d0-d12 dike injections, as discussed by *Grandin et al.* [2010b] [see also *Hamling et al.*, 2010]. Intrusion of dike d1 has induced a reduction of the magnitude of the normal tensile stress reaching −5 MPa in the region of emplacement of d1 and d11. Occurrence of subsequent dikes d2-d9 did not significantly change the magnitude of tensile stress in that region, because most of these dikes occurred more than 5 km to the south (Figure 1c). Dike d10 then induced an additional decrease of tension by −2 MPa in the d1-d11 area, again reducing the propensity for more dike intrusions there. Therefore, a cumulative decrease of background tension of −7 MPa occurred between June 2006 (prior to d1) and February 2009 (prior to d11) in the area where d1 and d11 were emplaced. The earthquakes accompanying the dike intrusions are likely to be related to slip on faults located in the vicinity and/or beyond the propagating crack tip [*Rubin*, 1992]. Slip on these faults is promoted by the stress perturbation induced by the crack tip (approximately the same for d1 and d11) and the

background tensile stress field (more tensile before d1 than before d11), explaining the lower seismic efficiency for d11 than for d1.

[40] Nevertheless, occurrence of dike intrusion d11 demonstrated that the stress state was still tensile in this area in February 2009. Observation of eruptions coeval with the two last observed dike intrusions of June 2009 (d12) and May 2010 (d13) may indicate that most of the tensile stress has now been relieved in the vicinity of the magma reservoir, thus increasing the likelihood for future eruptions there (Figure 1).

3.5. Time-Space Variation of Strain Energy Release

[41] As discussed above, earthquakes accompanying magma intrusion seem to migrate at a decaying velocity during dike growth. To infer the distribution of strain released by brittle seismic rupture as a function of time and space, we propose to follow the evolution of the cumulative Benioff strain release during propagation (Figure 6). When Benioff strain is plotted as a function of distance along the dikes from the source reservoir, we observe that strain release is not uniformly distributed spatially (Figures 7 and 8), and is neither correlated with the amount of opening along the dike body (Figure 1c). For dike d1, energy release as a function of dike length is triangular in shape, with the bulk of the energy released in two distinct peaks near the distal dike tip, and little seismicity near the region of first occurrence of seismicity, which likely corresponds to the point of magma injection from the source reservoir (Figures 7a–7c). The same first-order observation is repeated for d10 and d11, which also propagated toward the north (Figure 8d–8i). However, the triangular shape of seismic energy release with distance is less clear in the case of dike d10, mainly because two earthquakes of magnitude 4–4.5 occurred behind the crack front (i.e., near the midlength of the dike) after the end of propagation. Excluding these two shocks, a triangular shape of seismic energy released near the propagating dike front is also found.

[42] For the best constrained dike d9, seismicity is organized in two successive stages (Figures 8a–8c). First, a leading series of small magnitude earthquakes migrates rapidly away from the source. Then, a trail of earthquakes with larger magnitudes follows (Figure 8). The majority of seismic energy during intrusion of d9 was released at its southern extremity, but a significant fraction was also released near its injection point, mainly in the 4 h preceding onset of southward propagation of seismicity. The case of dike d2 is more difficult to interpret, as only 18 earthquakes are available for this dike, but the pattern of seismicity nevertheless resembles that of d9: accumulation of events near the entrance point, then a propagation of earthquakes, and finally sustained seismicity near the dike end.

[43] Overall, we notice that most of the seismic energy is released near the propagating tip of the dike, including in the period when the swarm has reached its final length. This indicates that little seismic energy is released along the dike body at any time, and that seismicity mostly reflects resistance involved in deforming host rock in a process zone surrounding the crack tip [*Ukawa and Tsukahara*, 1996; *Roman and Cashman*, 2006]. This confirms that perturbation of the ambient tensional stress field in the vicinity of the opening dike tip is capable of triggering seismicity, by raising the level of shear stress on optimally oriented faults located near the crack periphery [*Rubin*, 1992] (see also *Hayashi and Morita* [2003] for similar observations during a dike intrusion of 1998 in the Izu peninsula).

[44] Furthermore, simultaneous migration and growth of this process zone may explain other features of the distribution of seismic energy during dike propagation, such as the observed triangular shape of seismic energy release in the direction of migration, as shown in Figure 9. For a simple crack of length l loaded with a uniform driving pressure, Linear Elastic Fracture Mechanics (LEFM) predicts that the magnitude of maximum stress perturbation at distance r from the crack tip scales like $l^{1/2}$, with a decay proportional to $r^{-1/2}$ [e.g., *Rice*, 1968]. If we define the process zone as the region where stress conditions have been brought to the level defined by the shear failure envelope, then the size of the process zone may increase as l if off-dike irreversible deformation within the process zone is assumed to reflect damage of host rock in response to the stress singularity in the vicinity of the crack tip [*Andrews*, 1976; *Cowie and Scholz*, 1992; *Manighetti et al.*, 2004]. Alternatively, when fluid flow is considered, the damage zone could also scale with the length of the fluid lag zone behind the crack tip, which might increase quasi-linearly with l (so that process zone size is controlled by the fluid flow part of the problem and is not an intrinsic rock property) [*Rubin and Gillard*, 1998]. In both cases, the effect of dike propagation and growth results in the expansion of a region affected by crack tip–related seismicity, with the rate of seismic

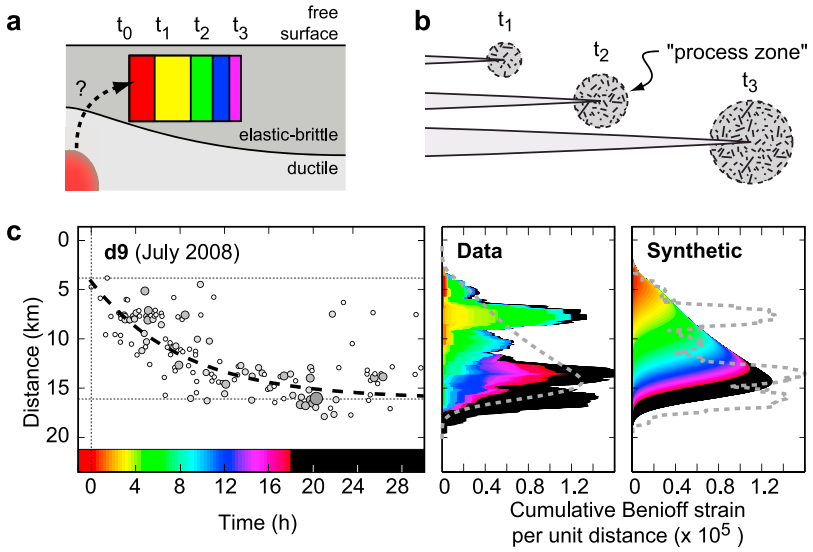

Figure 9. Synthetic model of seismic energy release for a dike propagating unidirectionally. (a) Intrusion of magma from a reservoir located beneath rift center into a dike located further down rift occurs horizontally. (b) The process zone around the propagating dike tip increases in size proportionally to dike length. (c) Example of (left) the migration of seismicity coeval to emplacement of dike d9, and (middle) observed and (right) synthetic distribution of cumulative Benioff strain as a function of time. The model is designed to cumulate seismic energy in a migrating region of increasing area, with a radius proportional to dike length and a rate of energy release proportional to migration velocity, using the exponential lengthening of the dike as a function of time (thick dashed curve on the first panel). Horizontal scale is arbitrary. Envelopes of observed and synthetic Benioff strain release (grey dashed curves) have been superimposed to facilitate comparison. Note that the model reproduces the first-order space-time distribution of strain release, which increases in magnitude during the migration. Second-order features, with peaks and troughs, are caused by spatial clustering of seismic activity, which are not taken into account in the model (see text for discussion).

energy released near the propagating dike front being proportional both to dike length and to the inflation rate of the dike, hence the velocity of propagation of the dike (Figure 9).

[45] Accordingly, this model assumes that the dike retains a constant shape during its growth. This is reasonable if fracture resistance is unimportant, and viscous pressure loss in the dike interior is low. However, this is not a good assumption if the shortest in-plane dimension is the dike height h. For the larger dikes in the MHR (e.g., d0 or d10) it seems likely that $l > h$. In that case, one could expect (given one of the above scenarios in which damage zone increases with dike size) the damage zone will increase with dike length l until l approaches h, at which point a steady state would probably be reached. Decrease of the pressure in the magma source may also lead to a variable length:thickness ratio during dike growth. Nevertheless, the model of migration and expansion of the process zone during dike growth may be still relevant to explain the first-order observation that little seismic energy is released in the first hour of the intrusions during the fast growth of the short dike, whereas more seismicity is generated in the later stages, when dike length increases at a slower rate.

[46] Alternatively, other mechanisms may explain the observed "triangular" increase of seismic moment release with distance from the source. One such mechanism is stopping of a dike due to inelastic deformation (e.g., fault slip, probably the clearest example of which was the first intrusion at Krafla in 1975 [*Björnsson*, 1985]). If so, one can expect significant seismicity at the distal end of the intrusion, and even continuing seismicity if fault slip and inflation by continued magma influx are coeval. In addition, one can expect a deeper brittle-ductile transition farther form the source, as supported by empirical evidence that (statistically) there are larger extensional tectonic stresses farther from the source (increase in fault scarp height in active rifts; increase in average dike thickness in eroded rifts [see *Rubin*, 1995; Grandin et al., submitted manuscript, 2011, and references therein]).

[47] In fact, both scenarios are plausible, and they may even combine in the following way: during

dike propagation away from the central reservoir, the dike tip moves toward a region where stress is closer to the failure envelope, or where a larger volume of rock is potentially near the failure envelope, and, simultaneously, the stress perturbation is progressively greater due to lengthening of the dike, hence generating more seismicity.

[48] Whichever interpretation is preferred, the lack of significant seismicity behind the crack front is clearly observed for the five dikes studied here. This first-order observation is compatible with (1) stress conditions being brought closer to lithostatic, and further from conditions for brittle rupture, off to the side of the dike body due to dike inflation and (2) deformation occurring above and below the dike during dike inflation in a largely aseismic fashion. The main deformation process at the base of the dike (~10 km) is likely to be ductile flow, due to the high temperature at that depth [e.g., *Benn et al.*, 1988]. Above the dike, slip on faults, associated with a substantial tensile component, which is abundantly described for the Manda Hararo dikes [*Rowland et al.*, 2007; *Grandin et al.*, 2009, 2010a], as well as in the Krafla rift [e.g., *Opheim and Gudmundsson*, 1989] and the Asal rift [e.g., *Doubre and Peltzer*, 2007], appears to occur mostly aseismically, presumably due to the combination of low confining stress conditions, and soft forcing exerted by the slowly inflating dike. Finally, the absence of seismic energy released near to the dike injection point during propagation/growth of the dike may support the hypothesis that stress conditions are nearly lithostatic there, possibly due to thermal weakening caused by the underlying midsegment focusing of melt and/or more frequent dike intrusions near the magma source (Grandin et al., submitted manuscript, 2011).

3.6. Multiple Dikes

[49] A key observation made during the 2005–present rifting episode in the MHR is that, in two instances (and probably three), a newly intruded dike has been emplaced at the same location as a previous dike in the sequence [*Grandin et al.*, 2010b]. These "multiple" events are d1 and d11 on the one hand, and d6 and d12 (and possibly d2), on the other (Figure 1c). Figure 10 shows the proportionality between the line-of-sight displacement fields induced by pairs d1-d11 and d6-d12, deduced from InSAR. The high coefficient of correlation between displacement fields suggests that variations in the strain field among the two pairs may be solely explained by the differing volumes of the dikes, while the geometry of the dikes was identical [*Grandin et al.*, 2010b]. In addition, seismicity associated with dike intrusions d1 and d11 indicates that the evolution of seismic energy release in time and space was very similar for the two dikes, with nearly equal migration velocities, bringing further support for the "multiple dike" hypothesis (Figures 7a–7c, Figures 8g–8i, Figure 6, and Table 1).

[50] Using a simple linear regression between the phase vectors, we find that the volume of dike d11 is about 62% of the volume of dike d1, whereas the volume of dike d12 is about 85% of the volume of d6 (Figures 10g–10i). This agrees well with volume fractions of 57% and 80% deduced from results of inversion of InSAR data for d1–d11 and d2–d12, respectively [*Grandin et al.*, 2010b]. Similarly, the volume of dike d6 represents nearly 120 % of the volume of d2. Resemblance between dikes d6 and d12 is also backed up by the observation that axial eruptions, associated with lava fountains, were emitted from nearly the same fissure system in the late phases of injection of these two dikes (red stars in Figure 1), with intrusion:extrusion volume ratios of 10:1 for d6, and 5:1 for d12 [*Ferguson et al.*, 2010; *Grandin et al.*, 2010b]. Similarity between d2 and d6 (and hence d12) is also suspected from the high coefficient of correlation between their phase vectors (Figure 10). Therefore, in spite of a lack of near-field seismological observation for dikes d6 and d12, one can extrapolate that the low migration velocity observed coeval with dike d2 is also a feature of dikes d6 and d12, and more generally, of small dike intrusions occurring in the vicinity of, or above the midsegment magma reservoir.

[51] Implications of the occurrence of such multiples are potentially important. As these dikes are emplaced in exactly the same sector of the plate boundary, to first order, the main difference between the first and second dike intrusion is the magnitude of tension on the plate boundary at the onset of the intrusion, which may have been significantly decreased due to previous dike intrusions in the sequence, as discussed earlier. However, one may wonder why the volumes of dikes d6 and d12 were the same, whereas the occurrence of an eruption coeval to dike d6 would have suggested that differential tensile stress had been completely relieved in its surroundings by the end of intrusion of d6 [*Arnott and Foulger*, 1994; *Buck et al.*, 2006]. If this were to be the case, dike d12 should have been entirely extrusive, as no more extensional tectonic

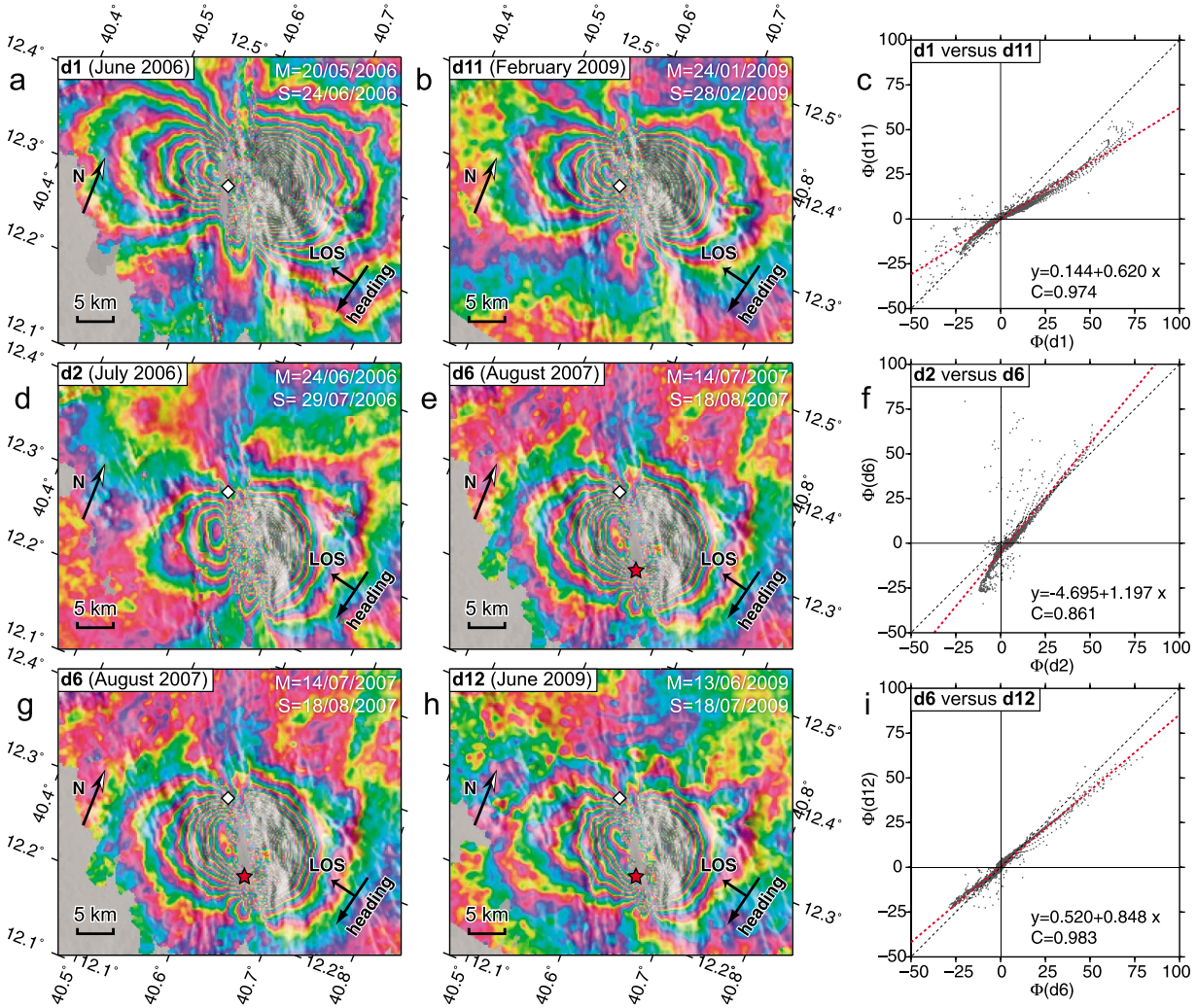

Figure 10. Comparison of Envisat InSAR line-of-sight (LOS) data for three pairs of multiple dikes: (a–c) d1 and d11, (d–f) d2 and d6, and (g–i) d6 and d12. Dates of acquisition of master (M) and slave (S) images are indicated at the upper right corner of each panel. Each fringe represents 2.8 cm of range change between the satellite and the ground. Look angle is from the right, with an incidence angle of ~40° with respect to vertical (track 464). Blue-red-yellow-green succession of fringes corresponds to increasing distance between the satellite and the ground (for more details on the processing of InSAR data, see *Grandin et al.* [2010b]). White diamond indicates the location of the caldera located at the summit of the axial depression. Red star indicates the location of fissural basaltic eruptions coeval with dikes d6 and d12. Figures 10c, 10f, and 10i show the distribution of LOS data (in cm) for one dike, plotted against LOS data for the other dike in the pair, on a pixel-by-pixel basis (i.e., d1 versus d11, d2 versus d6, and d6 versus d12). The red dashed line shows the linear regression for each multiple pair, and corresponding coefficient of correlation C is indicated on the bottom right of each graph. Black dashed line indicates a 1:1 ratio between phase vectors.

stress would have been available to drive dike opening.

[52] The answer may lie in the hypothesis of *Grandin et al.* [2010b], who calculated that, in the region of emplacement of dikes d6-d12 (2 km south of source reservoir, 2 km depth), the drop in tension associated with d12 on one hand, and the increase in tension by static stress transfer associated with the d7-d8-d9-d10-d11 sequence on the other hand, had competing contributions (−4 MPa *versus* + 3 MPa). This is due to the spatial configuration of successive dike intrusions d7 (November 2007) to d11 (February 2009), which have surrounded d6 (Figure 1c). Intrusion of a new dike there (d12) would have been required to return to lithostatic conditions in this area, and lead to a second eruption coeval to d12, suggest-

ing a "memory" of the system across several dike intrusions.

[53] Returning to the case of d1 and d11, the fact that increase of tension as a result of intrusions d2 to d10 has not produced the same effect as for the pair d6-d12, may be interpreted as indicating a significant magnitude of differential stress in the d1-d11 area, hence a lower sensitivity to perturbations by other dikes than the d6-d12 area. Since no eruption has been reported in this area prior to d13, we estimate that differential tensile stress in the d1-d11 area must have been at least twice the amount of tension drop coeval with dikes d1 and d11 (−3 MPa in each case) to be capable of preventing the occurrence of an eruption. Taking into account the fact that initial megadike d0 had already induced a tension drop nearly equal to the sum of the tension drops induced by d1 and d11, and that dike d0 has also contributed to releasing tensile stress in the area, this first estimate may be doubled, yielding a minimum value of 12 MPa for $\sigma_1 - \sigma_3$ in the d1-d11 area. Similarly, interpreting dikes d0a and d10 as multiple dikes [*Grandin et al.*, 2010b], and taking into account that they are the most voluminous dikes in the sequence (0.78 km^3 and 0.20 km^3, respectively), may imply that differential stress was even more tensile in the d0-d10 area (perhaps as much as 20 MPa or more) prior to onset of diking in September 2005. However, the occurrence of a new eruption near 12.34°N in May 2010 may indicate that this initial amount of differential tensile stress has now been nearly consumed, possibly suggesting that the maximum magnitude of the differential tensile stress in 2005 was near to 20 MPa at 8 km depth. Assuming that the maximum magnitude of differential tensile stress increases with depth at a rate of 10–15 MPa/km (Byerlee's law [e.g., *Brace and Kohlstedt*, 1980]), this is only 16–25 % of the limit imposed by brittle Mode II rupture of rocks. This suggests that dike intrusions reduce the level of tensile stress in a region of extension much more efficiently than normal faulting.

4. Conclusions

[54] The lateral dike injections in the Manda Hararo–Dabbahu Rift (MHR), studied from the perspective of the seismicity they induce, provide insights into the magmatic and tectonic processes responsible for crustal accretion in an environment similar to mid-ocean ridges (MOR). The five dikes discussed in this paper were fed from a single midsegment reservoir, located near 12.29°N, i.e., 7 km to the SSE from the topographic summit of the axial depression. Therefore, in the plate boundary setting of the MHR, the hypothesis of a topographic control on the directivity of lateral dike migrations [e.g., *Fialko and Rubin*, 1998] appears to be contradicted by evidence for lateral dike intrusions directed both up rift and down rift. Velocities of lateral migration of the dikes are in the same range as those deduced in the Krafla rift (Iceland) or slow spreading MOR (~1–2 km/h). The dikes that migrated up rift, toward the NNW, were generally more voluminous and emplaced at a faster velocity than the dikes that migrated toward the SSE. This suggests that differential tensile stress has a greater magnitude to the NNW than to the SSE of the central magma source. Variations in elastic thickness, or the history of past rifting episodes, may explain this difference, although this issue cannot be resolved currently.

[55] We found that dike-induced seismicity appears to be roughly concentrated near 5 km depth for the best-constrained dike of July 2008, which could suggest that seismicity occurs either at the depth of the dike or below the dike (depending on the confidence on estimated dike depth obtained by inversion of InSAR). Nevertheless, despite considerable uncertainty on hypocentral estimates due to the unfavorable network geometry, the time-space distribution of seismic energy release coeval with the dike intrusion is more compatible with seismicity being primarily released at the depth of the intrusion as a result of stress perturbation in the host rock near the propagating front of the magma-filled crack. After inception of the migration, little seismicity is detected behind the migrating front (1) off to the sides of the dike, (2) at its bottom, (3) in the subsurface above the dike, and (4) near the crack tail. Deformation during dike inflation/growth in these regions is likely to be aseismic, respectively due (1) to tensile stress being relieved, so that stress conditions are brought further from the limit imposed by criteria for brittle rupture, (2) to the ductile rheology of rocks at great depth, which prevents large preintrusion tensile stress accumulation, hence making the intrusion less likely to trigger seismicity, (3) to low confining pressure and slow forcing of subsurface faults, whose large cumulative slip is reached progressively as the dike inflates, possibly by aseismic creep with a substantial component of tensile opening, and (4) to nearly lithostatic stress conditions near the source reservoir, at the entrance point of magma in the brittle-elastic layer.

[56] In view of the volume of magma involved in the intrusions (0.05–0.2 km^3), seismic moment release during dike injections is very small (0.03–6.0 % of the geodetic moment release), probably due to the low differential tensile stress in the MHR. This feature may be typical of a mature MOR, where magmatism efficiently prevents accumulation of strong differential tensile stress. Seismic moment release is weakly correlated with dike volume and migration velocity, highlighting the additional influence of the rate of stress change in modulating the level of seismic energy released by dike injections.

[57] Nevertheless, dike-induced seismicity seems to be primarily sensitive to the magnitude of differential tensile stress in the region of dike emplacement, as suggested by the decrease of seismic energy released by successive dikes as the end of the current rifting episode is approaching. Based on a crude analysis of static stress changes associated with the 13 dike injections that occurred from 2005 to 2009 in the MHR, we estimate that the maximum differential tensile stress stored at the onset of the rifting episode in 2005 was ~20 MPa north of the source reservoir, at a depth of 8 km. This low magnitude of the differential stress suggests that dike intrusions operate at a lower level of tensile stress than is required for normal faulting, so that diking is more efficient than faulting to accommodate plate extension.

Acknowledgments

[58] This work would not have been possible without the constant support of the Institute of Geophysics, Space Science and Astronomy (IGSSA) of Addis Ababa University (AAU). In particular, Laike Asfaw, Tesfaye Kidane, and Elias Lewi are thanked for their support. We are grateful to Abebe Albie (IGSSA) and Yves Bertrand for their contribution to fieldwork. We thank Michael Asrat (IGSSA) for logistic assistance. François-Xavier Fauvelle and Éloi Fiquet are warmly thanked for the logistic support for fieldwork they provided through Centre Français des Études Éthiopiennes (CFEE), in Addis Ababa. Special thanks are addressed to our drivers from CFEE: Semenh Bacha, Amare Setotaw, and Temechach Yifru. Support from the authorities of the Afar regional government in Semera, particularly Idriss Mohamad, Mohammed Tahiro, and Mohammed Yayo, as well as Assefa Beyene and Adem Bori from Semera University, is acknowledged. Fruitful discussions with Mathilde Cannat, Benoît Taisne, and Steve Tait contributed to improve the paper. Exchanges of ideas and data with Manahloh Belachew, Laura Bennati, Roger Buck, Eric Calais, Cynthia Ebinger, Ian Hamling, Tim Wright, and Gezahegn Yirgu were also greatly appreciated. We thank two anonymous reviewers for their constructive comments on the paper. The acquisition of the seismic stations was possible thanks to support from Bonus Qualité Recherche (BQR) of Institut de Physique du Globe de Paris (IPGP) and support from the Volcanological Observatories of IPGP. Part of the resources for this work also originates from the funding of project Dynamics of Rifting in Afar (DoRA) by French's National Research Agency (ANR). DK was funded by NERC fellowship NE/E013945/1. We thank the European Space Agency (ESA) for programming the Envisat satellite and providing data used in this work (AOE-272, AOE-720). The Repeat Orbit Interferometry Package (ROI_PAC) software was provided by Caltech/Jet Propulsion Laboratory (JPL). The numerical implementation of the method of *Tarantola and Valette* [1982] was performed by Virginie Penquer'ch. Figures 1, 3, 5–10, and S1 were prepared with the Generic Mapping Tool (GMT) software [*Wessel and Smith*, 1991]. This is IPGP contribution 3142.

References

Abdallah, A., V. Courtillot, M. Kasser, A.-Y. Le Dain, J.-C. Lépine, B. Robineau, J.-C. Ruegg, P. Tapponnier, and A. Tarantola (1979), Relevance of Afar seismicity and volcanism to the mechanics of accreting plate boundaries, *Nature*, *282*, 17–23, doi:10.1038/282017a0.

Andrews, D. J. (1976), Rupture propagation with finite stress in antiplane strain, *J. Geophys. Res.*, *81*, 3575–3582, doi:10.1029/JB081i020p03575.

Arnott, S. K., and G. R. Foulger (1994), The Krafla spreading segment, Iceland. 2: The accretionary stress cycle and non-shear earthquake focal mechanisms, *J. Geophys. Res.*, *99*, 23,827, doi:10.1029/94JB00688.

Ayele, A., E. Jacques, M. Kassim, T. Kidane, A. Omar, S. Tait, A. Nercessian, J.-B. de Chabalier, and G. C. P. King (2007), The volcano seismic crisis in Afar, Ethiopia, starting September 2005, *Earth. Planet. Sci. Lett.*, *255*, 177–187, doi:10.1016/j.epsl.2006.12.014.

Ayele, A., D. Keir, C. J. Ebinger, G. Wright, T. J. Stuart, R. Buck, E. Jacques, G. Ogubazgh, and J. Sholan (2009), The September 2005 mega-dike emplacement in the Manda-Harraro nascent oceanic rift (Afar depression), *Geophys. Res. Lett.*, *36*, L20306, doi:10.1029/2009GL039605.

Baer, G., and Y. Hamiel (2010), Form and growth of an embryonic continental rift: InSAR observations and modelling of the 2009 western Arabia rifting episode, *Geophys. J. Int.*, *182*, 155–167, doi:10.1111/j.1365-246X.2010.04627.x.

Baer, G., Y. Hamiel, G. Shamir, and R. Nof (2008), Evolution of a magma-driven earthquake swarm and triggering of the nearby Oldoinyo Lengai eruption, as resolved by InSAR, ground observations and elastic modeling, East African Rift, 2007, *Earth. Planet. Sci. Lett.*, *272*, 339–352, doi:10.1016/j.epsl.2008.04.052.

Barisin, I., S. Leprince, B. Parsons, and T. Wright (2009), Surface displacements in the September 2005 Afar rifting event from satellite image matching: Asymmetric uplift and faulting, *Geophys. Res. Lett.*, *36*, L07301, doi:10.1029/2008GL036431.

Belachew, M., C. Ebinger, D. Cote, D. Keir, J. V. Rowland, J. O. S. Hammond, and A. Ayele (2011), Comparison of dike intrusions in an incipient seafloor-spreading segment

in Afar, Ethiopia: Seismicity perspectives, *J. Geophys. Res.*, doi:10.1029/2010JB007908, in press.

Benioff, B., and C. F. Richter (1951), Earthquakes and rock creep: (Part I: Creep characteristics of rocks and the origin of aftershocks), *Bull. Seismol. Soc. Am.*, *41*(1), 31–62.

Benn, K., A. Nicolas, and I. Reuber (1988), Mantle–crust transition zone and origin of wehrlitic magmas: Evidence from the Oman ophiolite, *Tectonophysics*, *151*, 75–85, doi:10.1016/0040-1951(88)90241-7.

Berckhemer, H., B. Baier, H. Bartelsen, A. Behle, H. Burkhardt, H. Gebrande, J. Makris, H. Menzel, H. Miller, and R. Vees (1975), Deep seismic soundings in the Afar region and on the highland of Ethiopia, in *Afar Depression of Ethiopia*, edited by A. Pilger and A. Rosier, pp. 89–107, Schweizerbart, Stuttgart, Germany.

Björnsson, A. (1985), Dynamics of crustal rifting in NE Iceland, *J. Geophys. Res.*, *90*, 10,151–10,162.

Blackman, D. K., C. E. Nishimura, and J. A. Orcutt (2000), Seismoacoustic recordings of a spreading episode on the Mohns Ridge, *J. Geophys. Res.*, *105*, 10,961–10,974, doi:10.1029/2000JB900011.

Brace, W. F., and D. L. Kohlstedt (1980), Limits on lithospheric stress imposed by laboratory experiments, *J. Geophys. Res.*, *85*, 6248–6252, doi:10.1029/JB085iB11p06248.

Brandsdóttir, B., and P. Einarsson (1979), Seismic activity associated with the September 1977 deflation of the Krafla central volcano in northeastern Iceland, *J. Volcanol. Geotherm. Res.*, *6*, 197–212.

Buck, W. R. (2006), The role of magma in the development of the Afro-Arabian Rift System, in *The Afar Volcanic Province Within the East African Rift System*, edited by G. Yirgu, C. J. Ebinger, and P. K. H. Maguire, *Geol. Soc. Spec. Publ.*, *259*, 43–54.

Buck, W. R., P. Einarsson, and B. Brandsdóttir (2006), Tectonic stress and magma chamber size as controls on dike propagation: Constraints from the 1975–1984 Krafla rifting episode, *J. Geophys. Res.*, *111*, B12404, doi:10.1029/2005JB003879.

Calais, E., et al. (2008), Strain accommodation by slow slip and dyking in a youthful continental rift, East Africa, *Nature*, *456*, 783–787, doi:10.1038/nature07478.

Callot, J., and L. Geoffroy (2004), Magma flow in the East Greenland dyke swarm inferred from study of anisotropy of magnetic susceptibility: Magmatic growth of a volcanic margin, *Geophys. J. Int.*, *159*, 816–830, doi:10.1111/j.1365-246X.2004.02426.x.

Cattin, R., C. Doubre, J. de Chabalier, G. King, C. Vigny, J. Avouac, and J. Ruegg (2005), Numerical modelling of quaternary deformation and post-rifting displacement in the Asal-Ghoubbet rift (Djibouti, Africa), *Earth. Planet. Sci. Lett.*, *239*, 352–367, doi:10.1016/j.epsl.2005.07.028.

Chatelain, P. (1978), Etude fine de la sismicité en zone de collision continentale au moyen dÕun réseau de stations portables: la région Hindu-Kush Pamir, Ph.D. thesis, Univ. de Grenoble I, Grenoble, France.

Cowie, P., and C. Scholz (1992), Physical explanation for the displacement-length relationship of faults using a post-yield fracture mechanics model, *J. Struct. Geol.*, *14*, 1133–1148, doi:10.1016/0191-8141(92)90065-5.

Curewitz, D., and A. Karson (1998), Geological consequences of dike intrusion at mid-ocean ridge spreading centers, in *Faulting and Magmatism at Mid-Ocean Ridges*, edited by W. R. Buck et al., pp. 117–136, AGU, Washington D. C.

Delaney, J. R., D. S. Kelley, M. D. Lilley, D. A. Butterfield, J. A. Baross, W. S. D. Wilcock, R. W. Embley, and M. Summit (1998), The quantum event of oceanic crustal accretion: Impacts of diking at mid-ocean ridges, *Science*, *281*, 222–230.

Dieterich, J., V. Cayol, and P. Okubo (2000), The use of earthquake rate changes as a stress meter at Kilauea volcano, *Nature*, *408*, 457–460.

Doubre, C., and G. Peltzer (2007), Fluid-controlled faulting process in the Asal Rift, Djibouti, from 8 yr of radar interferometry observations, *Geology*, *35*, 69–72, doi:10.1130/G23022A.1.

Doubre, C., I. Manighetti, C. Dorbath, L. Dorbath, D. Bertil, and J.-C. Delmond (2007a), Crustal structure and magmatotectonic processes in an active rift (Asal-Ghoubbet, Afar, East Africa): 2. Insights from the 23-year recording of seismicity since the last rifting event, *J. Geophys. Res.*, *112*, B05406, doi:10.1029/2006JB004333.

Doubre, C., I. Manighetti, C. Dorbath, L. Dorbath, E. Jacques, and J.-C. Delmond (2007b), Crustal structure and magmatotectonic processes in an active rift (Asal-Ghoubbet, Afar, East Africa): 1. Insights from a 5-month seismological experiment, *J. Geophys. Res.*, *112*, B05405, doi:10.1029/2005JB003940.

Doubre, C., et al. (2009), Dynamics of rifting in two active rift segments in Afar - Geodetic and Structural Studies - DoRA Project, *Eos Trans. AGU*, *90*(52), Fall Meet. Suppl., Abstract T31B-1817.

Dvorak, J. J., and A. T. Okamura (1987), A hydraulic model to explain variations in summit tilt rate at Kilauea and Mauna-Loa volcanoes, in *Volcanism in Hawaii*, *U.S. Geol. Surv. Prof. Pap.*, *1350*, 1281–1296.

Dziak, R. P., D. K. Smith, D. R. Bohnenstiehl, C. G. Fox, D. Desbruyeres, H. Matsumoto, M. Tolstoy, and D. J. Fornari (2004), Evidence of a recent magma dike intrusion at the slow spreading Lucky Strike segment, Mid-Atlantic Ridge, *J. Geophys. Res.*, *109*, B12102, doi:10.1029/2004JB003141.

Dziak, R. P., D. R. Bohnenstiehl, J. P. Cowen, E. T. Baker, K. H. Rubin, J. H. Haxel, and M. J. Fowler (2007), Rapid dike emplacement leads to eruptions and hydrothermal plume release during seafloor spreading events, *Geology*, *35*, 579–582.

Ebinger, C. J., D. Keir, A. Ayele, E. Calais, T. J. Wright, M. Belachew, J. O. S. Hammond, E. Campbell, and W. R. Buck (2008), Capturing magma intrusion and faulting processes during continental rupture: seismicity of the Dabbahu (Afar) rift, *Geophys. J. Int.*, *174*, 1138–1152, doi:10.1111/j.1365-246X.2008.03877.x.

Ebinger, C. J., A. Ayele, D. Keir, J. Rowland, G. Yirgu, T. J. Wright, and M. Belachew (2010), Length and timescales of rift faulting and magma intrusion: The Afar rifting cycle from 2005 to present, *Annu. Rev. Earth Planet. Sci.*, *38*, 439–466, doi:10.1146/annurev-earth-040809-152333.

Einarsson, P., and B. Brandsdóttir (1980), Seismological evidence for lateral magma intrusion during the July 1978 deflation of the Krafla volcano in NE-Iceland, *J. Volcanol. Geotherm. Res.*, *47*, 160–165.

Ferguson, D. J., T. D. Barnie, D. M. Pyle, C. Oppenheimer, G. Yirgu, E. Lewi, T. Kidane, S. Carn, and I. Hamling (2010), Recent rift-related volcanism in Afar, Ethiopia, *Earth. Planet. Sci. Lett.*, *292*(3–4), 409–418, doi:10.1016/j.epsl.2010.02.010.

Fialko, Y. A., and A. M. Rubin (1998), Thermodynamics of lateral dike propagation: Implications for crustal accretion at slow spreading mid-ocean ridges, *J. Geophys. Res.*, *103*, 2501–2514, doi:10.1029/97JB03105.

Foulger, G., and R. E. Long (1984), Anomalous focal mechanisms: Tensile crack formation on an accreting plate boundary, *Nature*, *310*, 43–45, doi:10.1038/310043a0.

Fox, C. G. (1995), Special collection on the June 1993 volcanic eruption on the CoAxial segment, Juan de Fuca Ridge, *Geophys. Res. Lett.*, *22*, 129–130, doi:10.1029/94GL02967.

Grandin, R., et al. (2009), September 2005 Manda Hararo-Dabbahu rifting event, Afar (Ethiopia): Constraints provided by geodetic data, *J. Geophys. Res.*, *114*, B08404, doi:10.1029/2008JB005843.

Grandin, R., A. Socquet, M. P. Doin, E. Jacques, J. B. De Chabalier, and G. C. P. King (2010a), Transient rift opening in response to multiple dike injections in the Manda Hararo rift (Afar, Ethiopia) imaged by time-dependent elastic inversion of interferometric synthetic aperture radar data, *J. Geophys. Res.*, *115*, B09403, doi:10.1029/2009JB006883.

Grandin, R., A. Socquet, E. Jacques, N. Mazzoni, J. B. De Chabalier, and G. C. P. King (2010b), Sequence of rifting in Afar (Manda-Hararo rift, Ethiopia, 2005–2009): Time-space evolution and interactions between dikes from InSAR and static stress change modeling, *J. Geophys. Res.*, *115*, B10413, doi:10.1029/2009JB000815.

Gutenberg, B., and C. F. Richter (1956), Earthquake magnitude, intensity, energy, and acceleration (second paper), *Bull. Seismol. Soc. Am.*, *46*(2), 105–145.

Hamling, I. J., A. Ayele, L. Bennati, E. Calais, C. J. Ebinger, D. Keir, E. Lewi, T. J. Wright, and G. Yirgu (2009), Geodetic observations of the ongoing Dabbahu rifting episode: new dyke intrusions in 2006 and 2007, *Geophys. J. Int.*, *178*, 989–1003, doi:10.1111/j.1365-246X.2009.04163.x.

Hamling, I. J., T. J. Wright, E. Calais, L. Bennati, and E. Lewi (2010), Stress transfer between thirteen successive dyke intrusions in Ethiopia, *Nat. Geosci.*, *3*, 713–717, doi:10.1038/ngeo967.

Hanks, T. C., and H. Kanamori (1979), A moment magnitude scale, *J. Geophys. Res.*, *84*, 2348–2350.

Hayashi, Y., and Y. Morita (2003), An image of a magma intrusion process inferred from precise hypocentral migrations of the earthquake swarm east of Izu Peninsula, *Geophys. J. Int.*, *153*, 159–174.

Hayward, N. J., and C. J. Ebinger (1996), Variations in the along-axis segmentation of the Afar Rift system, *Tectonics*, *15*, 244–257, doi:10.1029/95TC02292.

Hill, D. P. (1977), A model for earthquake swarms, *J. Geophys. Res.*, *82*, 1347–1352.

Hofstetter, R., and M. Beyth (2003), The Afar Depression: Interpretation of the 1960–2000 earthquakes, *Geophys. J. Int.*, *155*, 715–732, doi:10.1046/j.1365-246X.2003.02080.x.

Ida, Y. (1999), Effects of the crustal stress on the growth of dikes: Conditions of intrusion and extrusion of magma, *J. Geophys. Res.*, *104*, 17,897–17,910, doi:10.1029/1998JB900040.

Jacques, E., J.-C. Ruegg, J.-C. Lépine, P. Tapponnier, G. C. P. King, and A. Omar (1999), Relocation of $M \geq 2$ events of the 1989 Dôbi seismic sequence in Afar: evidence for earthquake migration, *Geophys. J. Int.*, *138*(2), 447–469, doi:10.1046/j.1365-246X.1999.00881.x.

Keir, D., et al. (2009), Evidence for focused magmatic accretion at segment centers from lateral dike injections captured beneath the Red Sea rift in Afar, *Geology*, *37*(1), 59–62, doi:10.1130/g25147a.1.

Keir, D., M. Belachew, C. Ebinger, J. M. Kendall, J. O. S. Hammond, G. W. Stuart, A. Ayele, and J. V. Rowland (2011), Mapping the evolving strain field during continental breakup in the Afar Depression, *Nat. Commun.*, in press.

Klein, F. W., R. Y. Koyanagi, J. S. Nakata, and W. R. Tanigawa (1987), The seismicity of Kilauea's magma system, in *Volcanism in Hawaii*, *U.S. Geol. Surv. Prof. Pap.*, *1350*, 1019–1186.

Lee, W. H., and J. C. Lahr (1975), HYPO71 (revised): a computer program for determining hypocenter, magnitude, and first motion pattern of local earthquakes, *U.S. Geol. Surv. Open File Rep., 75-311*.

Lengliné, O., D. Marsan, J.-L. Got, V. Pinel, V. Ferrazzini, and P. G. Okubo (2008), Seismicity and deformation induced by magma accumulation at three basaltic volcanoes, *J. Geophys. Res.*, *113*, B12305, doi:10.1029/2008JB005937.

Lin, J., G. M. Purdy, H. Schouten, J.-C. Sempere, and C. Zervas (1990), Evidence from gravity data for focused magmatic accretion along the Mid-Atlantic Ridge, *Nature*, *344*, 627–632, doi:10.1038/344627a0.

Lister, J. R., and R. C. Kerr (1991), Fluid-mechanical models of crack propagation and their application to magma transport in dykes, *J. Geophys. Res.*, *96*, 10,049–10,077.

MacDonald, K. C., D. S. Scheirer, and S. M. Carbotte (1991), Mid-ocean ridges–Discontinuities, segments and giant cracks, *Science*, *253*, 986–994, doi:10.1126/science.253.5023.986.

Magde, L. S., D. W. Sparks, and R. S. Detrick (1997), The relationship between buoyant mantle flow, melt migration, and gravity bullÕs eyes at the Mid-Atlantic Ridge between 33°N and 35°N, *Earth. Planet. Sci. Lett.*, *148*, 59–67, doi:10.1016/S0012-821X(97)00039-3.

Manighetti, I., G. King, and C. G. Sammis (2004), The role of off-fault damage in the evolution of normal faults, *Earth. Planet. Sci. Lett.*, *217*, 399–408, doi:10.1016/S0012-821X(03)00601-0.

Mériaux, C., and C. Jaupart (1995), Simple fluid dynamic models of volcanic rift zones, *Earth. Planet. Sci. Lett.*, *136*, 223–240, doi:10.1016/0012-821X(95)00170-H.

Mohamed, K. (2009), Fonctionnement sismique du Golfe de Tadjoura: Approches statistique (1973–2007) et deterministe (cas de la squence 2004), Ph.D. thesis, Inst. de Phys. du Globe de Paris, Paris.

Nooner, S. L., L. Bennati, E. Calais, I. J. Hamling, T. J. Wright, W. R. Buck, and E. Lewi (2009), Post-rifting relaxation in the Afar region, Ethiopia, *Geophys. Res. Lett.*, *36*, L21308, doi:10.1029/2009GL040502.

Opheim, J. A., and A. Gudmundsson (1989), Formation and geometry of fractures, and related volcanism, of the Krafla fissure swarm, Northeast Iceland, *Geol. Soc. Am. Bull*, *101*(12), 1608–1622.

Pallister, J. S., W. A. McCausland, S. Jónsson, Z. Lu, H. M. Zahran, S. E. Hadidy, A. Aburukbah, I. C. F. Stewart, P. R. Lundgren, R. A. White, and M. R. H. Moufti (2010), Broad accommodation of rift-related extension recorded by dyke intrusion in Saudi Arabia, *Nat. Geosci.*, *3*, 705–712, doi:10.1038/ngeo966.

Pedersen, R., F. Sigmundsson, and P. Einarsson (2007), Controlling factors on earthquake swarms associated with magmatic intrusions; Constraints from Iceland, *J. Volcanol. Geotherm. Res.*, *162*, 73–80, doi:10.1016/j.jvolgeores.2006.12.010.

Pollard, D. D., and P. Segall (1987), Theoretical displacements and stresses near fractures in rock: with applications to faults, joints, veins, dikes, and solution surfaces, in *Fracture Mechanics of Rock*, edited by B. K. Atkinson, pp. 277–349, Academic, London.

Pollard, D. D., P. T. Delaney, W. A. Duffield, E. T. Endo, and A. T. Okamura (1983), Surface deformation in volcanic rift

zones, *Tectonophysics*, *94*(1–2), 541–584, doi:10.1016/0040-1951(83)90034-3.

Real, C. R., and T.-L. Teng (1973), Local Richter magnitude and total signal duration in southern California, *Bull. Seismol. Soc. Am.*, *63*(5), 1809–1827.

Rice, J. R. (1968), A path independent integral and the approximate analysis of strain concentration by notches and cracks, *J. Appl. Mech.*, *35*, 379–386.

Richter, C. F. (1958), *Elementary Seismology*, 578 pp., edited by W. H. Freeman, San Francisco, Calif.

Rivalta, E. (2010), Evidence that coupling to magma chambers controls the volume history and velocity of laterally propagating intrusions, *J. Geophys. Res.*, *115*, B07203, doi:10.1029/2009JB006922.

Roman, D. C., and K. V. Cashman (2006), The origin of volcano-tectonic earthquake swarms, *Geology*, *34*, 457–460, doi:10.1130/G22269.1.

Rowland, J. V., E. Baker, C. J. Ebinger, D. Keir, T. Kidane, J. Biggs, N. Hayward, and T. J. Wright (2007), Fault growth at a nascent slow-spreading ridge: 2005 Dabbahu rifting episode, Afar, *Geophys. J. Int.*, *171*(10), 1226–1246, doi:10.1111/j.1365-246X.2007.03584.x.

Rubin, A. M. (1992), Dike-induced faulting and graben subsidence in volcanic rift zones, *J. Geophys. Res.*, *97*, 1839–1858, doi:10.1029/91JB02170.

Rubin, A. M. (1995), Propagation of magma-filled cracks, *Annu. Rev. Earth Planet. Sci.*, *23*, 287–336, doi:10.1146/annurev.ea.23.050195.001443.

Rubin, A. M., and D. Gillard (1998), Dike-induced earthquakes: Theoretical considerations, *J. Geophys. Res.*, *103*, 10,017–10,030, doi:10.1029/97JB03514.

Rubin, A. M., and D. D. Pollard (1987), Origins of Blade-Like Dikes in Volcanic Rift Zones, in *Volcanism in Hawaii*, *U.S. Geol. Surv. Prof. Pap.*, 1350, 1449–1470.

Ruegg, J.-C., M. Kasser, J.-C. Lépine, and A. Tarantola (1979), Geodetic measurements of rifting associated with a seismo-volcanic crisis in afar, *Geophys. Res. Lett.*, *6*, 817–820.

Smith, D. K., and J. R. Cann (1999), Constructing the upper crust of the Mid-Atlantic Ridge: A reinterpretation based on the Puna Ridge, Kilauea Volcano, *J. Geophys. Res.*, *104*, 25,379–25,400, doi:10.1029/1999JB900177.

Solomon, S. C., P. Y. Huang, and L. Meinke (1988), The seismic moment budget of slowly spreading ridges, *Nature*, *334*, 58–60, doi:10.1038/334058a0.

Spence, D. A., and D. L. Turcotte (1985), Magma-driven propagation of cracks, *J. Geophys. Res.*, *90*, 575–580, doi:10.1029/JB090iB01p00575.

Sykes, L. R. (1970), Earthquake swarms and sea-floor spreading, *J. Geophys. Res.*, *75*, 6598–6611, doi:10.1029/JB075i032p06598.

Taisne, B., and S. Tait (2009), Eruption versus intrusion? Arrest of propagation of constant volume, buoyant, liquid-filled cracks in an elastic, brittle host, *J. Geophys. Res.*, *114*, B06202, doi:10.1029/2009JB006297.

Tarantola, A., and B. Valette (1982), Inverse Problems = Quest for Information, *J. Geophys.*, *50*, 159–170.

Toda, S., R. S. Stein, and T. Sagiya (2002), Evidence from the AD 2000 Izu islands earthquake swarm that stressing rate governs seismicity, *Nature*, *419*, 58–61.

Tolstoy, M., D. R. Bohnenstiehl, M. H. Edwards, and G. J. Kurras (2001), Seismic character of volcanic activity at the ultraslow-spreading Gakkel Ridge, *Geology*, *29*, 1139–1142, doi:10.1130/0091-7613(2001)029.

Tolstoy, M., J. P. Cowen, E. T. Baker, D. J. Fornari, K. H. Rubin, T. M. Shank, F. Waldhauser, D. R. Bohnenstiehl, D. W. Forsyth, R. C. Holmes, B. Love, M. R. Perfit, R. T. Weekly, S. A. Soule, and B. Glazer (2006), A sea-floor spreading event captured by seismometers, *Science*, *314*, 1920–1922, doi:10.1126/science.1133950.

Tryggvason, E. (1984), Widening of the Krafla fissure swarm during the 1975–1981 volcano-tectonic episode, *Bull. Volcanol.*, *47*(1), 47–69, doi:10.1007/BF01960540.

Ukawa, M., and H. Tsukahara (1996), Earthquake swarms and dike intrusions off the east coast of Izu Peninsula, central Japan, *Tectonophysics*, *253*, 285–303, doi:10.1016/0040-1951(95)00077-1.

Wessel, P., and W. H. F. Smith (1991), Free software helps map and display data, *Eos Trans. AGU*, *72*, 441–441, doi:10.1029/90EO00319.

Whitehead, J. A., H. J. B. Dick, and H. Schouten (1984), A mechanism for magmatic accretion under spreading centres, *Nature*, *312*, 146–148.

Wright, T. J., C. Ebinger, J. Biggs, A. Ayele, G. J. Yirgu, D. Keir, and A. Stork (2006), Magma-maintained rift segmentation at continental rupture in the 2005 Afar dyking episode, *Nature*, *442*, 291–294, doi:10.1038/nature04978.

Yirgu, G., A. Ayele, and D. Ayalew (2006), Recent seismo-volcanic crisis in Northern Afar, Ethiopia, *Eos Trans. AGU*, *87*(33), 325–329, doi:10.1029/2006EO330001.